Cell Systems

Article

Phased fragility and stability of non-genetic B cell states in the germinal center accelerate the genetic evolution of antibodies

Graphical abstract

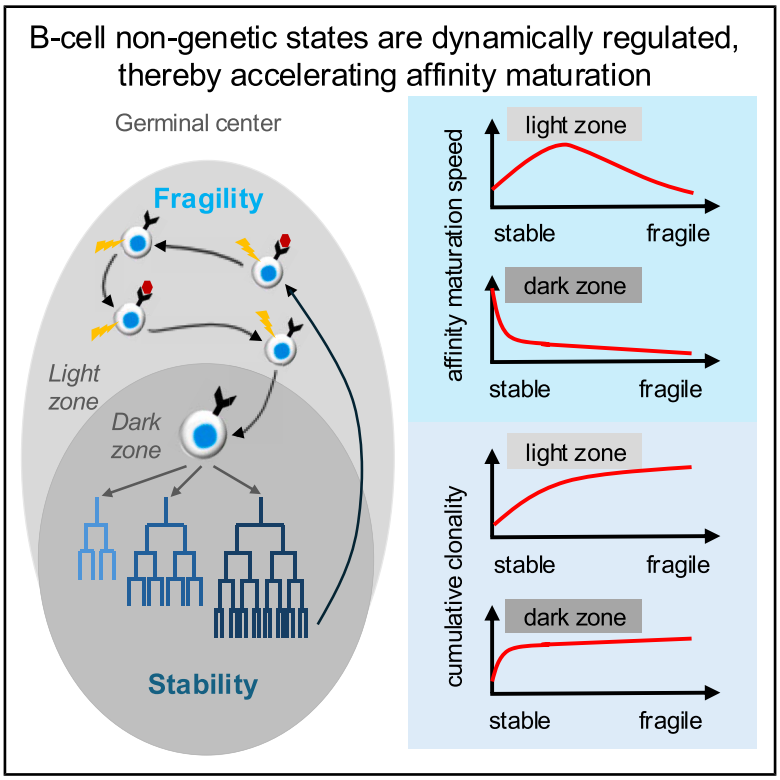

Authors

Mark Y. Xiang,
Haripriya Vaidehi Narayanan,
Vaibhava Kesarwani,
Rohan Vanheusden, Tiffany Wang,
Alexander Hoffmann

Correspondence

ahoffmann@ucla.edu

In brief

Xiang et al. present a mathematical model of Darwinian antibody affinity maturation—validated in mouse mutant immunization studies—to examine the impact of variable non-genetic cell states. They report optimal antibody maturation with some stochasticity during affinity selection but high non-genetic state heritability during the clonal burst phase.

Highlights

- Clonal selection theory posits that B cells make affinity-dependent fate decisions
- A math model reveals that stochasticity in selection can speed affinity maturation
- In contrast, during clonal bursts, highly heritable non-genetic states are optimal
- This model correctly predicts emergent vaccine response properties in mouse mutants

Xiang et al., 2026, Cell Systems *17*, 101590
June 17, 2026
https://doi.org/10.1016/j.cels.2026.101590

CellPress

Cell Systems

CellPress
OPEN ACCESS

Article

Phased fragility and stability of non-genetic B cell states in the germinal center accelerate the genetic evolution of antibodies

Mark Y. Xiang,[1,2,3,5] Haripriya Vaidehi Narayanan,[1,2,5] Vaibhava Kesarwani,[1] Rohan Vanheusden,[1,4] Tiffany Wang,[1] and Alexander Hoffmann[1,2,6,7,*]

[1]Institute for Quantitative and Computational Biosciences, University of California, Los Angeles, Los Angeles, CA, USA
[2]Department of Microbiology, Immunology, and Molecular Genetics, University of California, Los Angeles, Los Angeles, CA, USA
[3]Bioinformatics Program, University of California, Los Angeles, Los Angeles, CA, USA
[4]Systems Biology Program, University of California, Los Angeles, Los Angeles, CA 90095, USA
[5]These authors contributed equally
[6]Senior author
[7]Lead contact
*Correspondence: ahoffmann@ucla.edu
https://doi.org/10.1016/j.cels.2026.101590

SUMMARY

Vaccine responses depend on the Darwinian genetic evolution of B cells to generate high-affinity antibodies. However, B cells gain non-genetic heterogeneity while searching for antigen and T helper cells, but then their non-genetic cell states remain stable within proliferative clonal bursts. We explored the functional consequence of this dynamic control of non-genetic variability by developing a mathematical model, integrating a wealth of immunological knowledge. We discovered that variability in B cell fate decisions does not impair but instead accelerates affinity maturation by allowing high-affinity outliers to escape plasma cell differentiation and seed further rounds of Darwinian evolution. During clonal bursts, non-genetic cell state stability further promotes their amplification. The resulting model correctly predicts emergent vaccine response properties in mouse strains with altered B cell fate decision profiles. Our work reconciles classical B cell clonal selection theory with the experimentally observed non-genetic variability, and it provides an interpretable knowledge-based modeling framework to support personalized vaccination strategies.

INTRODUCTION

With the identification of DNA as the carrier of genetic information that provides for the heritable traits of organisms,[1] Conrad Waddington coined the term epigenetics to refer to the set of instructions that act on top of genetic instructions to explain how distinct cell types emerge despite identical genomes during development.[2] These instructions are heritable within a cell lineage but may gradually change or bifurcate during differentiation, thereby forming the Waddington landscape.[3] Yet, recent studies have revealed that the set of non-genetic instructions—contained in cells' chromatin states,[4] molecular regulatory networks,[5] and subcellular organization[6]—exhibits substantial heterogeneity even among genetically identical cells. Unlike genetic mutations, which cause stable changes to the genetic instructions, non-genetic states are dynamic and may respond to environmental cues and molecular stochastic fluctuations. For example, following inheritance of the same non-genetic state, sibling cancer cells rapidly diverge in their propensity to respond to a death-inducing ligand.[7]

In the immune system—where cellular responses must balance robustness with precision—such non-genetic variability introduces both opportunity and challenges, potentially contributing to population resilience through bet-hedging.[8] However, in processes that depend on reliable cell decision-making, non-genetic variability may be detrimental. For example, the stimulus-response specificity of innate immune sentinel cells is diminished by variable responses to defined stimuli.[9,10] Further, in Darwinian processes that aim for the selection of genetic instructions that confer the greatest fitness, unreliable fate decision-making is potentially detrimental. The generation of high affinity antibody by B cells involves a Darwinian process of mutation and selection as described by classical clonal selection theory.[11] Thus, the discovery of heterogeneous B cell responses to identical stimulation *in vitro* was notable[12,13] and prompted the development of population dynamics models that assumed stochastic decision-making.[14,15] Pedigree lineage tracing through microscopy revealed that non-genetic cell states were actually remarkably stable within stimulus-induced proliferative bursts and that the observed heterogeneity was largely due to non-genetic differences in the starting population.[16] Yet, it remains unknown how this dynamically regulated non-genetic variability affects the selection and production of high-affinity antibodies *in vivo*.

Please cite this article in press as: Xiang et al., Phased fragility and stability of non-genetic B cell states in the germinal center accelerate the genetic evolution of antibodies, Cell Systems (2026), https://doi.org/10.1016/j.cels.2026.101590

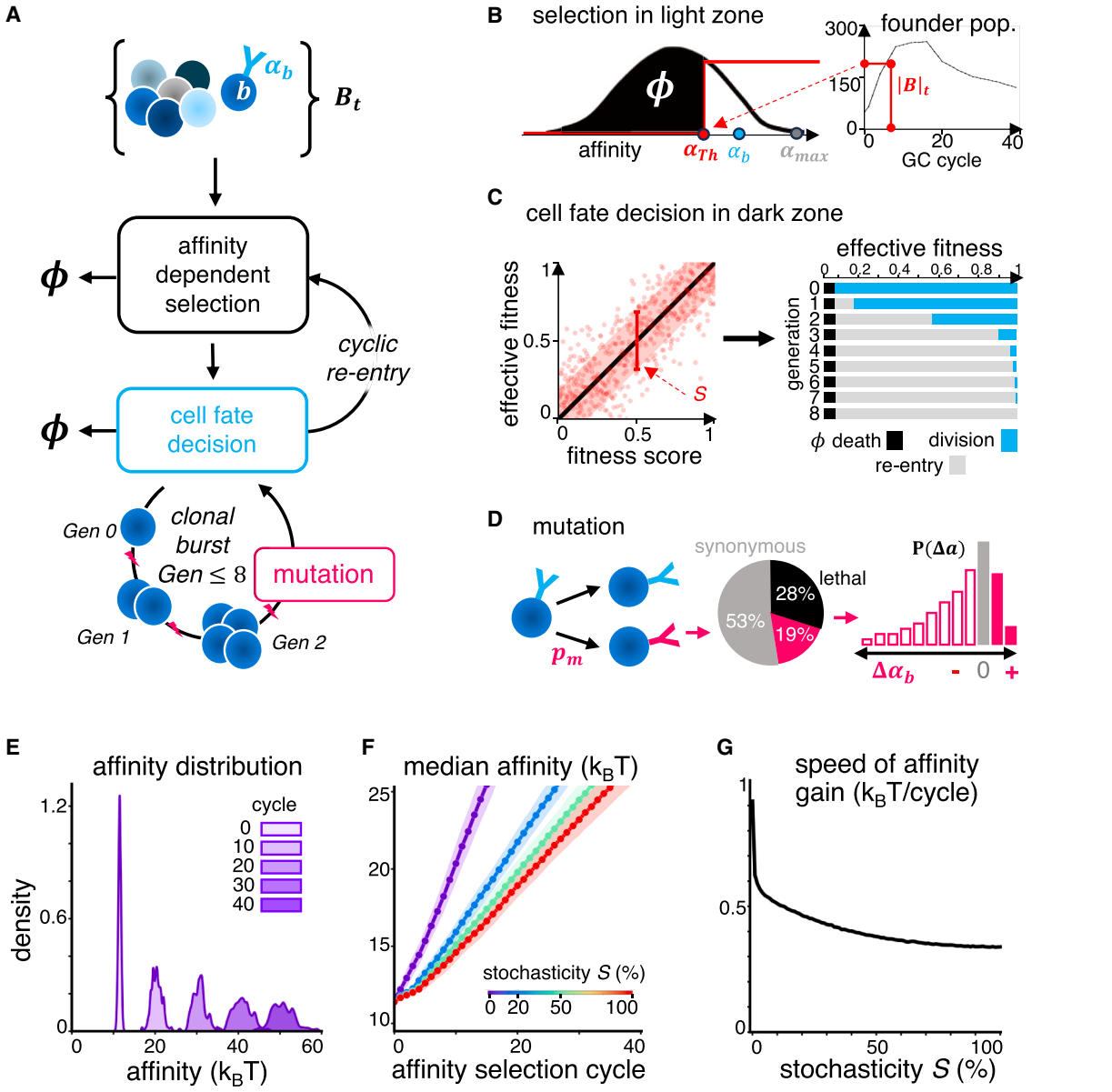

Figure 1. A mathematical model of the Darwinian process underlying antibody generation suggests that stochastic B cell fate decisions are detrimental to affinity gain

(A) Schematic of the mathematical model of affinity maturation incorporating stochasticity in cell fate decision-making.[23–33] The model includes sequential processes of affinity-dependent selection in the LZ and cell fate decisions in the DZ across multiple affinity maturation cycles, with mutation occurring during proliferative bursts in the DZs. α_b represents the B cell receptor (BCR) or antibody affinity in a given B cell *b*, B_t represents the population of B cells at any given cycle, and ϕ represents the removal of B cells due to death.

(B) Schematic of parameterizing affinity-dependent selection in the LZ. Based on the size of the GC (right), we define the affinity threshold α_{th} that selects a given number of highest-affinity B cells. This threshold varies dynamically across cycles, due to changes in both GC size and the B cell affinity distribution.[34]

(C) Schematic of parameterizing affinity-dependent but stochastic cell fate decisions in the DZ. (Left) Stochastic cell fate decisions are modeled using a stochasticity parameter *S* to distribute affinity-dependent fitness scores. See also Figure S6. (Right) The resulting effective fitness scores are used to determine the corresponding B cell fate decisions, using a generation-specific probabilistic cell fate map. Higher fitness scores correspond to more proliferation, while lower fitness scores favor cell death, consistent with affinity-dependent clonal selection theory.[11,35]

(D) Schematic of parameterizing mutation and affinity changes during proliferative bursts in the DZ. During each cell division, each daughter cell independently mutates its B cell receptor with a probability p_m, set at 0.5 based on literature.[36,37] The pie chart indicates the proportion of synonymous (gray), lethal (black), and non-synonymous (magenta) mutations.[38] For the fraction of non-synonymous mutations, the histogram represents the probability of changes in B cell affinity, where gray indicates no change, open bars indicate detrimental mutations, and shaded bars indicate affinity-enhancing mutations.[39] $\Delta\alpha_b$ represents the antibody affinity change in the given B cell *b* during a non-synonymous mutation, with the "−" sign (open bars) on the left indicating a decrease in affinity and the "+" sign (solid bars) on the right an increase in affinity.

(legend continued on next page)

Please cite this article in press as: Xiang et al., Phased fragility and stability of non-genetic B cell states in the germinal center accelerate the genetic evolution of antibodies, Cell Systems (2026), https://doi.org/10.1016/j.cels.2026.101590

In the antibody response to vaccination, B cells migrate between two compartments within the lymph node's germinal center (GC): the light zone (LZ), where they undergo selection by picking up antigen and identify cognate T cells to provide pro-proliferative signals, and the dark zone (DZ), where they proliferate over several divisions and mutate their antibody genes before cycling back to the LZ. Over a 2-week vaccine response time, there are estimated to be up to 40 GC cycles of selection and proliferation/mutation.[17,18] In the LZ, B cells—primarily in the G0/G1 cell-cycle phase—encounter numerous signals that impinge on their molecular networks[19] and may generate a highly heterogeneous set of non-genetic states. In contrast, B cells in the DZ undergo rapid proliferation via shortened or absent G1 phases[20] and largely preserve their non-genetic state. Indeed, upon analyzing single B cells from the LZ and DZ in both mouse and human GCs,[21,22] we found that LZ B cells show a looser clustering in gene expression space with more cells at greater distances from the centroid (Figures S1A and S1B), a higher entropy indicating diversity of cell states (Figure S1C), as well as a greater number of genes showing heterogeneous expression above a variability threshold (Figure S1D). This increased transcriptomic variability in LZ B cells compared with DZ B cells is consistent with an underlying epigenetic cause for their observed heterogeneity in gene expression. Thus, the GC reaction cycles between two phases of the non-genetic cell state: fragility in the LZ and relative stability in the DZ. This provides a natural framework to investigate how dynamical modulation of cell-intrinsic variability may shape immune outcomes.

Here, we addressed the question of how the dynamic control of non-genetic variability of B cells impacts the vaccine antibody response. Rather than focusing on the molecular details, our goal was to theoretically dissect how the stochasticity and heritability of B cell fate decisions shapes affinity maturation. As there are no experimental tools to manipulate non-genetic variability in defined ways, we developed a mathematical model of the antibody maturation process in the GC by leveraging a wealth of immunological knowledge before validating it with experimental perturbation studies in mouse mutants. This model encodes key aspects of classical clonal selection theory: experimental measurements of cell numbers; GC characteristics; antibody mutation rates; selection stringency; and the heterogeneous fate decisions of cell death, proliferation, and differentiation. By manipulating the dynamic control of the non-genetic cell-state fragility (stochasticity) or its stability (heritability), we discovered how the phased fragility and stability of B cell non-genetic states do not impair but accelerate the evolution of high-affinity B cells. Our findings offer a conceptual framework for understanding how phased non-genetic variability modulates immune evolution, with implications for vaccine design and the interpretation of clonal diversity in B cell response.

RESULTS

A knowledge-based mathematical model of B cell affinity maturation

To study how non-genetic heterogeneity of B cells affects the genetic evolution of their antibody gene sequences that drives their affinity maturation, we leveraged extensive prior knowledge[23–31] to construct a mathematical model of the Darwinian process of B cell selection and clonal expansion in GCs (Figure 1A). We parametrized the initial B cell population size based on the number of clones seeding a typical GC,[32] starting with a distribution of low antigen affinities.[33] We abstracted the spatial segregation of the GC into LZ and DZ and the B cell migration between them into sequentially occurring processes within each zone. The model incorporates repeated cycles of three core processes: affinity-dependent selection in the LZ, followed by stimulus-dependent cell fate decisions to survive, proliferate, or differentiate in the DZ, with mutation during proliferative clonal bursts.

During affinity-dependent selection, either the initial founder B cells or their progeny re-entering subsequent cycles after a clonal burst are positively selected based on a dynamic affinity threshold[40] (Figure 1B left). This is a result of competition for limited T cell help[41] and shifts with time,[40] reflecting the carrying capacity of the GC, which expands in size before gradually contracting[34] (Figure 1B right). Low-affinity B cells that fail selection undergo apoptosis, while the surviving high-affinity B cells proceed to cell fate decisions.

In contrast to models that assign stochastic B cell fates based on expected outcomes,[26,27,42] this model assigns affinity-dependent fate decisions as prescribed by classical clonal selection theory.[11] For each B cell that is positively selected, a fitness score is assigned corresponding to the rank of its affinity within the population, as a proxy for signaling by T follicular helper cells. Fitness scores are then mapped onto cell fate decisions described by a multi-generational cell fate map that conforms to classical clonal selection theory[43] and literature measurements[44,45] (Figure 1C right; see STAR Methods for details and illustrations). To capture the non-genetic heterogeneity in B cell proliferation, we introduced a stochasticity parameter S that describes the degree of decorrelation between a cell's initial affinity-dependent fitness score and the actual cell fate decisions made in successive generations of a proliferative burst (Figure 1C left; see STAR Methods for details and illustrations).

To complete the Darwinian process, we modeled the generation of genetic variants—B cells undergoing division activate somatic hypermutation, which alters the receptor's affinity for the antigen based on the probability of mutation occurrence[36–38] and the probability that the mutation results in a change in affinity versus being detrimental (cell death) or neutral (no change in affinity or fitness)[39] (Figure 1D). We ensured reproducibility in the probabilistic formulations of cellular behaviors by performing sufficient Monte Carlo simulations to achieve 95% confidence within a 1% margin of error

(E) Kernel density plots showing the distribution of affinities of all B cells re-entering the subsequent GC selection cycle, at regular intervals during affinity maturation when cell fate stochasticity is set to zero. Note the heavy tail that contains cells driving the affinity gain through the Darwinian process.
(F and G) Line plots of (F) the median affinity and (G) the speed of affinity gain (defined as the increase in median affinity relative to the previous selection cycle) for B cells re-entering each subsequent affinity maturation cycle, across varying degrees of cell fate stochasticity with rainbow color in linear scale. Points indicate the median, and shaded regions indicate the 95% confidence interval across 100 simulation runs, except (G) where stochasticity parameter varied from 1% to 100% in 1% increments, and each was evaluated over 2,000 Monte Carlo simulations to ensure statistical robustness.

Please cite this article in press as: Xiang et al., Phased fragility and stability of non-genetic B cell states in the germinal center accelerate the genetic evolution of antibodies, Cell Systems (2026), https://doi.org/10.1016/j.cels.2026.101590

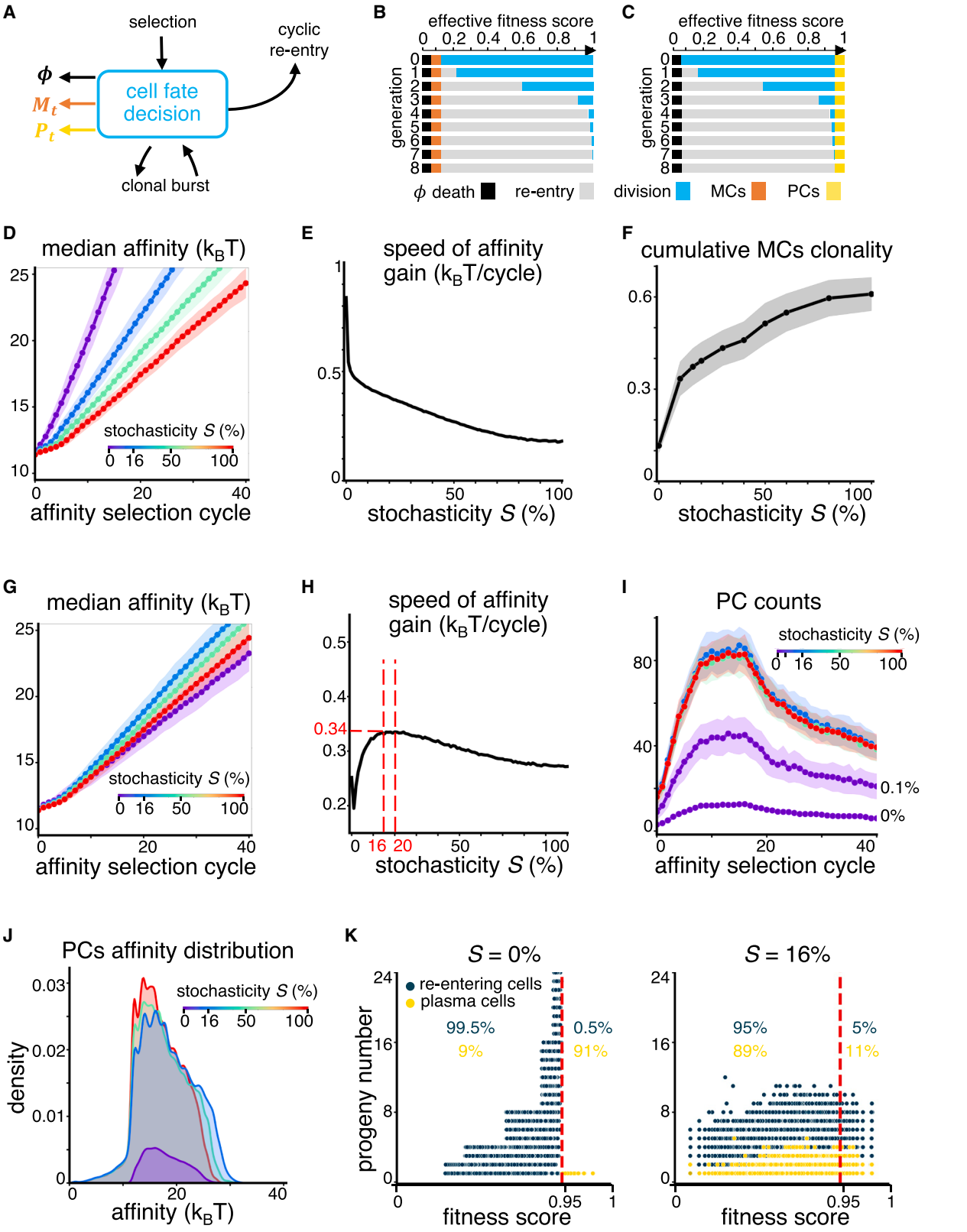

(legend on next page)

of the median estimate. First simulations of the model with these literature-derived parameters (Table 1) showed that, as expected for a Darwinian process, antibody affinity increases over time (Figure 1E), demonstrating the capacity to simulate affinity maturation as a function of the key regulatory steps described in clonal selection theory when parameterized by a wealth of published experimental data. Affinity distributions were characterized by a tail of high-affinity outliers that became more pronounced at later cycles (Figure 1E), indicating that affinity maturation is an outlier-driven process.

Simplest model: Stochasticity in B cell fate decisions impairs affinity gain

Prior *in vitro* studies of B cell proliferation revealed a high degree of non-genetic cell-to-cell heterogeneity in proliferative responses[13,14] such that probabilistic cell fate decision models could capture the heterogeneous population dynamics.[46] With the newly established model, we could now investigate the impact of this probabilistic cell fate decision process (Table 2) on antibody affinity maturation. Simulations showed that with increasing stochasticity S, the gain in median affinity is dramatically reduced (Figure 1F), as the tail of high-affinity outliers in later cycles is diminished. Quantifying the rate of affinity gain as a function of the stochasticity parameter confirmed this conclusion (Figure 1G).

Thus, our simplest model of Darwinian evolution predicted that the generation of non-genetic heterogeneity in the propensity of cell fate decision making, a fundamental hallmark of cell biology, substantially impairs the speed of affinity maturation. However, B cell biology in the GC reaction involves two additional fate decision events to be considered: differentiation into memory B cells and antibody-producing plasma cells.

Considering memory B cell differentiation: Stochasticity improves clonal diversity

Low-affinity B cells give rise to memory B cells that may seed future antigen responses, while high-affinity B cells differentiate into antibody-secreting plasma cells.[35,47] We refined the model by incorporating differentiation into memory B cells or plasma cells as additional cell fate decisions (Figures 2A–2C). This allows us to contrast the removal of GC B cells from the Darwinian evolutionary process at either end of their affinity distribution.

While the lowest affinity B cells are eliminated by death, we modeled the next 5% of B cells at low affinity differentiating into memory B cells[49–51] (Figure 2B). We then explored how stochasticity in cell fate decisions affects affinity maturation when low-affinity variants are removed. As earlier, we found that increasing stochasticity substantially reduces the affinity gains of cycling GC B cells (Figures 2D and 2E) and hence memory B cells sampled from this pool (Figure S2A). However, stochasticity dramatically improves the clonal diversity of memory B cells (Figure 2F) and their total numbers produced (Figure S2B), although at the expense of mutational depth (Figure S2C).

Considering plasma cell differentiation: Stochasticity enhances affinity gain

We again revised the cell fate map based on literature measurements[25,44,45,48] without memory differentiation but with the 5% of B cells at the highest affinities expected to differentiate into plasma cells (Figure 2C). We again explored how stochasticity in cell fate decisions affects gains in the affinity of plasma cells.

Increasing the stochasticity parameter from 0% to 100% revealed that the relationship between stochasticity and the affinity maturation rate is no longer monotonic when high-affinity outliers are removed as plasma cells (Figure 2G). Specifically, we observed an optimal level of stochasticity (between 15% and 25%, peaking at ~16%) at which cycling GC B cells showed the fastest affinity maturation speed (Figure 2H). We confirmed this by analyzing the affinity distribution of plasma cells, which displayed similar trends in maturation dynamics (Figures S2D and S2E).

Our results indicated that similarly to memory B cells, stochasticity in cell fate decisions dramatically increases the total number of plasma cells (sampled from the large pool of GC B cells), and this effect persists even at high levels of stochasticity (Figure S2F). Likewise, increasing stochasticity also improved

Figure 2. Considering memory and plasma cell differentiation, an optimal degree of stochasticity in B cell fate decisions emerges

(A) Schematic of modified cell fate decision module incorporating memory B cell M_t and plasma cell differentiation P_t.[11,35] See also Figure S6.

(B) Schematic of the modified cell fate decision map, directing the 5% of B cells just above the lowest effective fitness scores (undergoing cell death) in each generation to differentiate into memory B cells.[25,48]

(C) Schematic of the modified cell fate decision map, directing B cells with the top 5% of effective fitness scores in each generation to differentiate into plasma cells.[25,48] As in Figure 1C, effective fitness scores of founders and progeny in each cycle are distributed as specified by the stochasticity parameter S.

(D–F) Line plots of (D) the median affinity of cycling GC B cells re-entering the LZ for a subsequent round of selection, (E) their speed of affinity gain (defined as the increase in median affinity relative to the previous selection cycle), and (F) the cumulative clonal diversity of memory B cells (defined as fraction of extant clones relative to number of founder B cell clones seeding the GC at cycle 0) generated in each affinity maturation cycle, for varying degrees of cell fate stochasticity. Points indicate the median, and shaded regions indicate the 95% confidence interval across 100 simulation runs, except (E) where the stochasticity parameter was varied from 1% to 100% in 1% increments, and each was evaluated over 2,000 Monte Carlo simulations to ensure statistical robustness.

(G–I) Line plots of (G) the median affinity of cycling GC B cells re-entering the LZ for a subsequent round of selection, (H) their speed of affinity gain (defined as the increase in median affinity relative to the previous selection cycle), and (I) the total number of plasma cells with high affinity (defined as above 20.7 k_BT or K_D 1 nM) generated in each affinity maturation cycle, for varying degrees of cell fate stochasticity with rainbow color in linear scale. Points indicate the median, and shaded regions indicate the 95% confidence interval across 100 simulation runs, except (H) where the stochasticity parameter was varied from 1% to 100% in 1% increments, and each was evaluated over 2,000 Monte Carlo simulations to ensure statistical robustness. The vertical red lines in (H) indicate the region where speed of affinity gain is highest, between 16% and 20% stochasticity.

(J) Kernel density plots showing the distribution of plasma cell affinities generated at different degrees of cell fate stochasticity with rainbow color in linear scale.

(K) Progeny plot showing the number of GC-reentering cells (blue dots) and plasma cells (yellow dots) that derive from a single progenitor whose affinity-dependent fitness score is shown on x axis (cycle 21). The red line indicates the 5% fitness score cutoff for plasma cell differentiation.[25,48] Percentages indicate the fraction of re-entering cells (blue) and plasma cells (yellow) that are below and above this fitness score cutoff.

See also Figure S2.

Please cite this article in press as: Xiang et al., Phased fragility and stability of non-genetic B cell states in the germinal center accelerate the genetic evolution of antibodies, Cell Systems (2026), https://doi.org/10.1016/j.cels.2026.101590

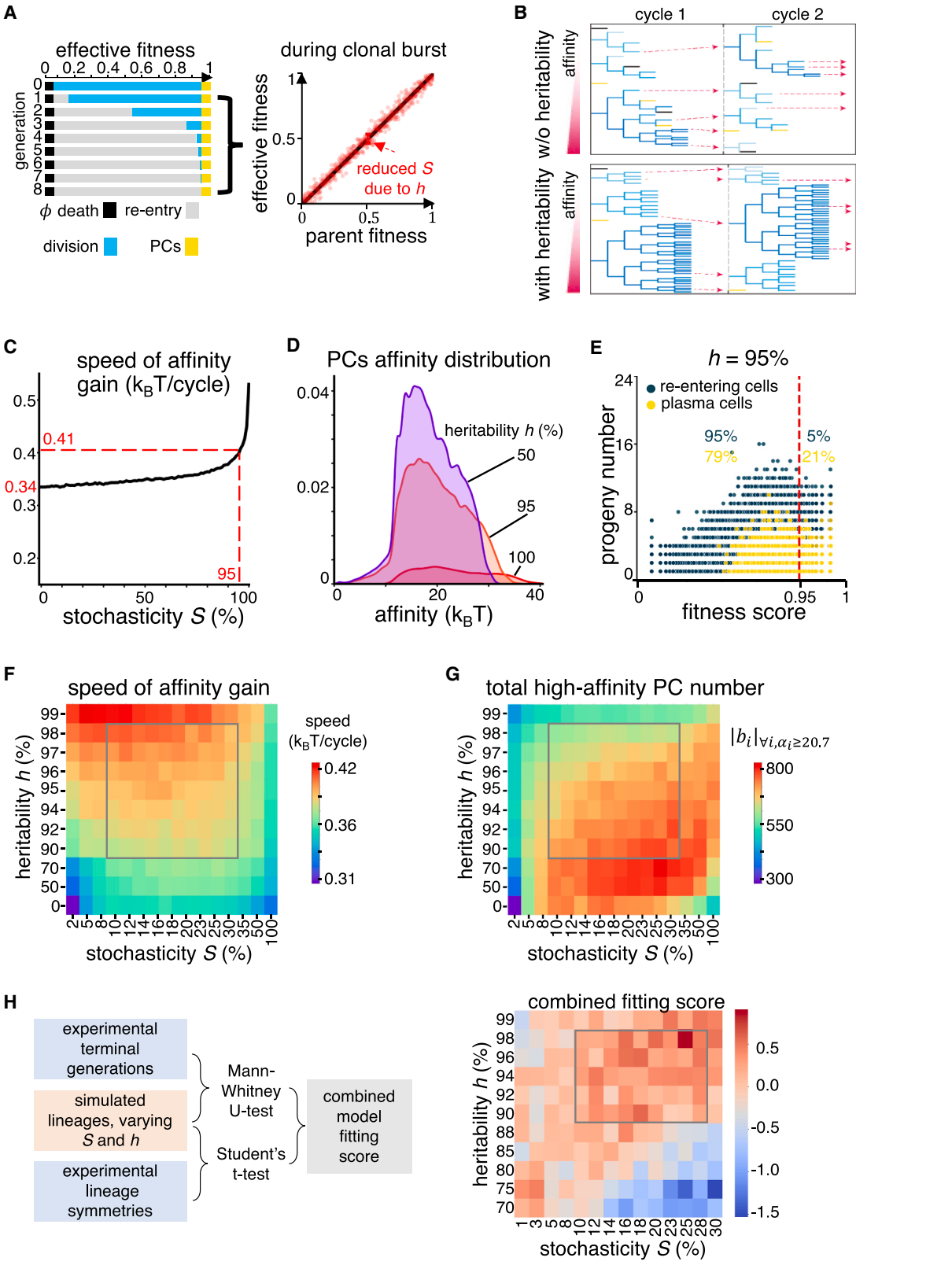

Figure 3. Phased stochasticity and heritability of B cell fate decisions enables both rapid affinity gains and high plasma cell counts

(A) Schematic showing generation-specific cell fate map (left) with reduced stochasticity *S* due to heritability *h* (right, due to heritability) for progeny in generation 1 onward of a proliferative burst as observed by live-cell microscopy.[16] See also Figure S6.

(legend continued on next page)

Please cite this article in press as: Xiang et al., Phased fragility and stability of non-genetic B cell states in the germinal center accelerate the genetic evolution of antibodies, Cell Systems (2026), https://doi.org/10.1016/j.cels.2026.101590

clonal diversity of plasma cells (Figures S2G and S2H) while diminishing their mutational depth (Figure S2I). However, plotting plasma cell affinities revealed that only the moderate level of stochasticity (16%) yields the largest proportion of high-affinity plasma cells (Figure 2I), i.e., increases the tail of high-affinity outliers in the distribution of their affinities (Figure 2J). This suggests that moderate stochasticity may optimize affinity maturation by balancing plasma cell differentiation with progeny production among high-affinity cells.

To further investigate how stochasticity could result in a gain in affinity maturation, we examined the progeny of selected cells that are either differentiating into plasma cells or re-entering the GC for another evolutionary cycle (Figure 2K). At 0% stochasticity, all highest-affinity cells differentiate into plasma cells without any further proliferative expansion, while almost all cells re-entering selection (99.5%) are below the high-affinity threshold. However, at the optimal 16% stochasticity, there is a 5% tail of high-affinity cells that complete the proliferative program to enter another round of selection and may therefore contribute to subsequent cycles of selection and mutation. Also, while only 11% of all plasma cells now cross the high-affinity threshold, their total numbers have been amplified by division prior to differentiation.

In other words, stochasticity in cell fate decisions allows some high-affinity cells to escape removal from the Darwinian process, thereby accelerating affinity maturation gains. Yet, stochasticity also allows lower-affinity B cells to become plasma cells, reducing the stringency of affinity-dependent differentiation. Thus, as stochasticity increases, its detrimental impact on affinity-based selection dominates over the benefit. This results in an optimal level of stochasticity in cell fate decisions for efficient affinity maturation that improves both the affinity and clonal diversity of plasma cells.

Within-burst heritability of non-genetic states stabilizes proliferative fitness

Following selection in the LZ, B cells undergo a clonal burst of rapid, successive divisions over multiple generations in the DZ. Live-cell microscopy of stimulus-induced B cell proliferation revealed that sibling and cousin cells make highly correlated cell fate decisions, suggesting that the wide heterogeneity of B cell responses to selection signals (via the B cell receptor [BCR] and CD40) is in fact based on heterogeneous non-genetic cell states in selected cells that are largely inherited by the progeny within a clonal burst.[16] The stability of these non-genetic cell states of proliferating B cells stands in contrast to their relative instability in a cancer cell line, where correlations between cell death decisions of siblings are lost within hours.[7]

Expanding the model to account for within-burst heritability of the non-genetic cell state, we examined how it might shape B cell proliferation dynamics in the GC and the maturation of antibody affinity. Specifically, we introduced a heritability parameter that reduces stochasticity during the successive generations within a clonal burst, allowing us to study its effects (Figure 3A; see STAR Methods for details and illustrations). We could thereby generate lineage trees with and without within-burst heritability. Without heritability of the non-genetic cell state, progeny cells made fully independent fate decisions, generating asymmetric trees (Figure 3B top). By contrast, high heritability (95%) led to a more cohesive symmetric lineage structure (Figure 3B bottom), where sibling cells made highly correlated cell fate decisions in line with experimental observations.[16]

We then explored how within-burst heritability in the model impacts affinity maturation in the plasma cell population, at the previously identified optimal value of 16% stochasticity. Unlike the stochasticity in cell fate decisions, within-burst heritability of fate decision propensities showed a monotonic, although non-linear, gain accelerating affinity maturation (Figure S3A). The speed of affinity gains increased dramatically within the biologically relevant range (Figure 3C), suggesting an evolutionary benefit for maintaining the non-genetic cell state during a clonal burst.

Our results also indicated that high within-burst heritability reduced the total number of plasma cells (Figure S3B), while promoting higher affinity (Figure S3C), as observed in the plasma cell affinity distribution (Figure 3D). This implies a trade-off between plasma cell production and affinity gain. To further understand this, we assessed progeny counts of founder cells, distinguishing between those differentiating into plasma cells and those re-entering the GC LZ. We found that high heritability restricts the affinity threshold for plasma cell formation, increasing the proportion of plasma cells above the high-affinity

(B) Example lineage trees across two successive selection cycles, at optimal 16% stochasticity modified by a heritability parameter of 0% (top) or 95% (bottom) within proliferative bursts. In each generation, dead cells are indicated in black, proliferating cells in shades of blue, and plasma cells in yellow. Pink arrows show cells re-entering the next selection cycle.
(C) Line plot of the speed of affinity gain (defined as the difference between median plasma cell affinities generated in the current and previous selection cycles), for optimal 16% cell fate stochasticity among founder B cells but varying degrees of heritability during proliferative bursts. Points indicate the median, and shaded regions indicate the 95% confidence interval where the stochasticity parameter was varied from 1% to 100% in 1% increments, and each was evaluated over 2,000 Monte Carlo simulations to ensure statistical robustness. The red lines indicate the rise in speed of affinity gain from 0% to 95% heritability.
(D) Kernel density plots showing distribution of plasma cell affinities generated at different degrees of heritability and optimal 16% cell fate stochasticity.
(E) Progeny plot showing the number of GC-reentering cells (blue dots) and plasma cells (yellow dots) that derive from a single progenitor whose affinity-dependent fitness score is shown on *x* axis (cycle 21). The red line indicates the 5% fitness score cutoff for plasma cell differentiation.[25,48] Numbers indicate the fraction of re-entering cells (blue) and plasma cells (yellow) that are below and above this fitness score cutoff.
(F and G) Two-dimensional heatmap of (F) the speed of affinity gain and (G) total number of plasma cells above the high-affinity threshold of 20.7 k_BT (corresponding to K_D 1 nM)[33] across varying degrees of both stochasticity and heritability in B cell fate decisions. (Left) Workflow for estimating the stochasticity and heritability of B cells using experimental data of tracked single WT B cell lineages from proliferative bursts *in vitro*.[16] (Right) Heatmap of the resulting model fitting scores across stochasticity and heritability, with higher scores indicating better fits to the experimental data. In (F)–(H), every heatmap pixel represents the median of 100 simulation runs (300 runs for H), and the gray boxes outline the physiologically plausible range of values for stochasticity and heritability based on experimental observations.[16]
See also Figure S3.

Please cite this article in press as: Xiang et al., Phased fragility and stability of non-genetic B cell states in the germinal center accelerate the genetic evolution of antibodies, Cell Systems (2026), https://doi.org/10.1016/j.cels.2026.101590

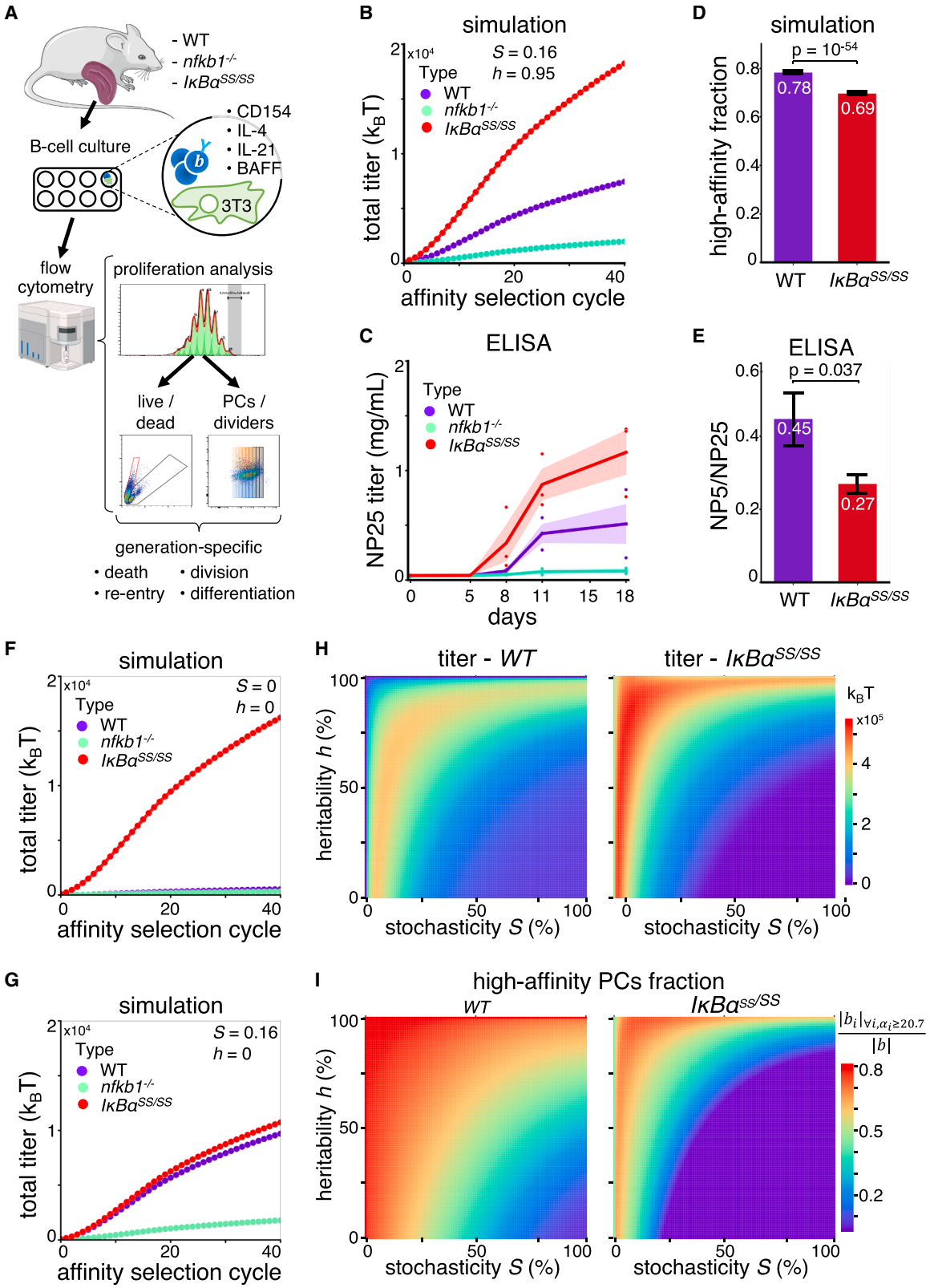

(legend on next page)

threshold—from 11% high-affinity plasma cells without any heritability to 21% high-affinity plasma cells at 95% heritability (Figure 3E).

Dynamic regulation of non-genetic variability optimizes affinity maturation

We extended our analysis to examine the combined effects of stochasticity in cell fate decisions and within-burst heritability. We found that the greatest speed of affinity gain occurs at moderate stochasticity (5%–25%) and very high heritability levels (95%–99%; Figure S3H shows full parameter range, with Figure 3F magnifying the region of interest), consistent with results from individual parameter analyses (Figures 2D and 3C). As expected, at a fixed stochasticity or heritability value, varying the other parameter confirmed previous findings. However, the number of high-affinity plasma cells showed a different pattern, with a sharp decline at both extremely low stochasticity and very high heritability (Figure S3I). Moderate values for both stochasticity and heritability create a broad parameter range for increased plasma cell counts, peaking at a different optimum with similarly moderate stochasticity (around 10%–25%) but only intermediate values of heritability (50%–70%; Figure 3G). This reiterates that some stochasticity is indispensable for effective affinity maturation, while heritability modulates a trade-off between plasma cell numbers and affinities.

We then evaluated how the predicted optima for stochasticity and heritability correspond with experimental observations by comparing the outcomes of our simulations with our previously published experimental observations[16] (Figure 3H). We estimated the stochasticity in proliferative bursts by comparing the spread of terminal generations with those observed in dye dilution assays[13,16] and heritability by assessing the cell fate lineage symmetry to traces from single-cell live microscopy assays[16] under identical stimulus conditions. By iteratively comparing the experimentally measured distributions of terminal generations and lineage symmetry with model simulations that independently varied both parameters, we estimated the best-fit between simulations and experiments at moderate stochasticity between 12% and 28% and high heritability between 90% and 98%, consistent with our previous predictions for maximizing affinity gain.

We also compared the effects of stochasticity (Figures S2C–S2F) and heritability (Figures S3D–S3G) on the clonality and mutational depth of plasma and memory cells, as additional dimensions of the GC response. We found that heritability had a modest but opposite effect to stochasticity. At higher heritability, increased progeny within a given lineage led to more mutations, while the number of clones selected at a given carrying capacity is restricted.

Taken together, non-genetic heterogeneity among founder B cells and its within-burst heritability balance the multidimensional properties of speed of affinity gain, titer, clonality, and mutational depth, defining a biological set point for the antibody response. The congruence between predicted and experimentally fitted stochasticity and heritability parameters underscores the role of phasing the fragility and stability of the non-genetic cell state in optimizing production and maturation of high-affinity plasma cells, supporting an effective immune response.

Predicting and testing emergent properties of vaccine responses in distinct mouse strains

B cell fate decision-making propensities are determined by molecular regulatory mechanisms that may differ between individuals due to genetics or health status, while non-genetic variability distributes these fate decisions. We asked whether our model incorporating the phasing of non-genetic variability could predict vaccination response outcomes based on B cell fate decision propensities.

We experimentally tested model predictions of affinity maturation through perturbation studies using genetically modified mice.

Figure 4. Key B cell biological parameters in cell fate decision-making determine trade-offs in vaccine-responsive affinity maturation outcomes

(A) Schematic of workflow to generate probabilistic cell fate maps from *in vitro* B cell culture for three genotypes (WT, *nfkb1*$^{-/-}$, *IκBα*$^{SS/SS}$) (where SS indicates an allele present in Sjögren's syndrome) varying in cell fate propensities. Follicular B cells from naive mouse spleens are cultured on a stromal layer of 3T3 fibroblasts with pro-survival B cell activating factor (BAFF) and a median (non-saturating) dose of T-dependent stimuli (CD154, interleukin [IL]-4, IL-21), to mimic the GC microenvironment while ensuring uniform stimulation and consistency with prior studies of proliferative heterogeneity. Proportions undergoing different cell fates within each generation are assessed at 120 h by flow cytometry.

(B) Model-predicted binding antibody titers (estimated as the cumulative plasma cell affinities) in each of the three genotypes, based on probabilistic cell fate maps generated from the *in vitro* flow cytometry measurements, with 16% stochasticity and 95% heritability corresponding to both theoretical optima and statistical fits to physiological data. Each point represents the median titer value across 100 simulation runs.

(C) Line plots of *in vivo* serum antibody titers measured by ELISA against NP_{25} in mice from each genotype immunized with NP_{21}-OVA. Each dot represents a measurement from one mouse, with solid lines showing the mean and shaded regions showing the standard error across three biological replicates for each genotype.

(D) Bar chart of predicted high-affinity antibody fractions relative to total titer, estimated as the ratio of cumulative plasma cell affinities for those above 20.7 k_BT (corresponding to K_D 1 nM)[33] versus the whole population, in WT and *IκBα*$^{SS/SS}$ genotypes using measurements from days 11 to 18, with 16% stochasticity and 95% heritability corresponding to both theoretical optima and fit to physiological data. Error bars represent standard errors across 100 simulation runs for each genotype. Differences between bars are statistically significant with p value 10^{-54} by a Students' t test.

(E) Measured high-affinity antibody fractions in WT and *IκBα*$^{SS/SS}$ genotypes, evaluated as the ratio of antibody binding to NP_5 (stringent, high-affinity titer) versus NP_{25} (total titer). Error bars show standard errors across three biological replicates per genotype. Differences between bars are statistically significant with p value 0.037 by a Students' t test.

(F and G) Simulations of alternative parameter combinations of (F) 0% stochasticity corresponding to the deterministic clonal selection theory and (G) 16% stochasticity and 0% heritability corresponding to the Cyton model. Each point represents the median titer value across 100 simulation runs.

(H and I) Heatmaps of the (H) titer and (I) high-affinity plasma cell fraction across the full range of stochasticity and heritability parameters in 1% increments for both WT and *IκBα*$^{SS/SS}$ mutants, using the corresponding experimentally derived cell fate maps. Each parameter combination was evaluated over 2,000 Monte Carlo simulations to ensure statistical robustness.

See also Figure S4.

Please cite this article in press as: Xiang et al., Phased fragility and stability of non-genetic B cell states in the germinal center accelerate the genetic evolution of antibodies, Cell Systems (2026), https://doi.org/10.1016/j.cels.2026.101590

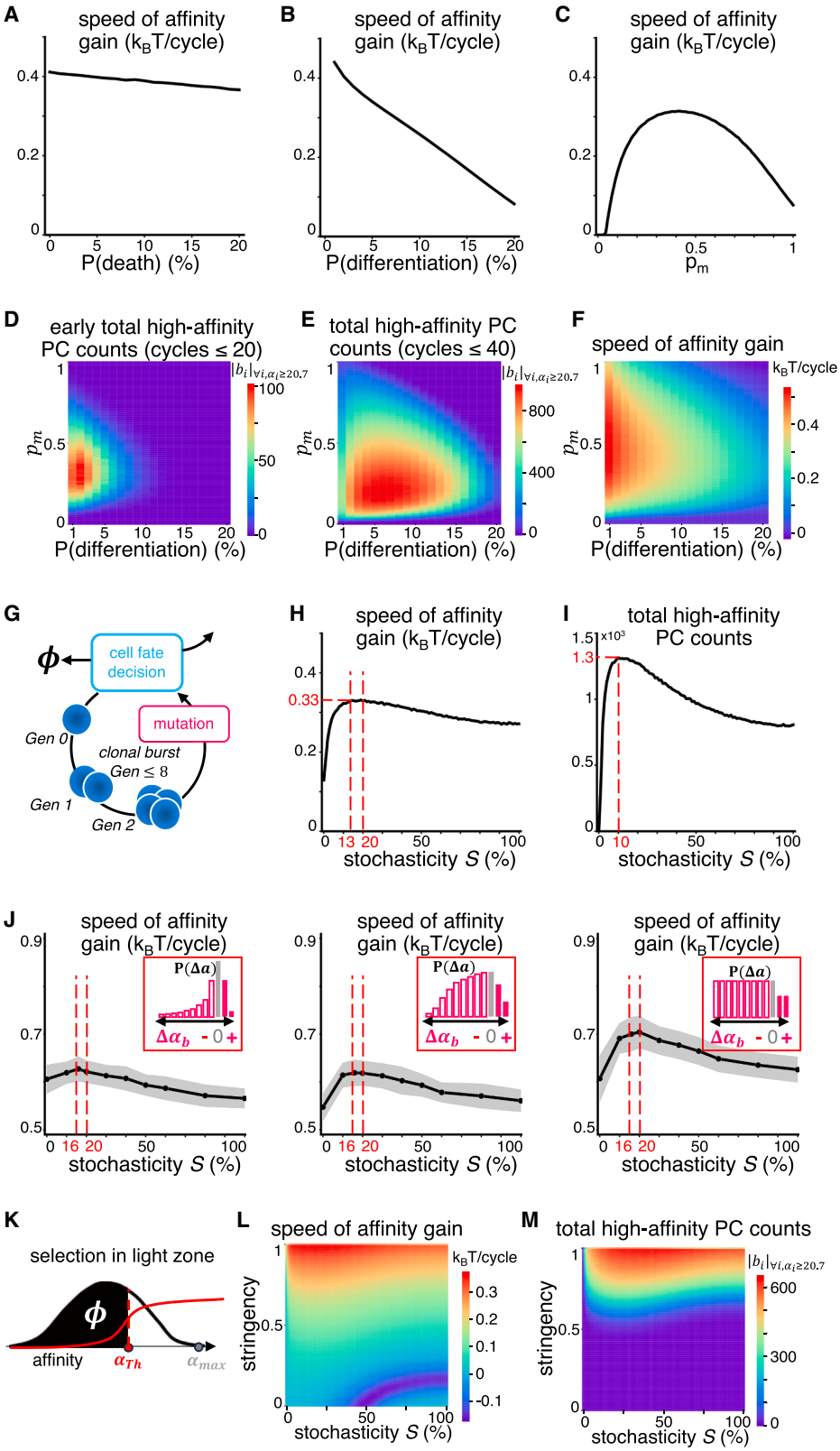

(legend on next page)

In response to stimulation in the GC by antigen and T follicular helper cells, the nuclear factor κB (NF-κB) signaling network is the key regulatory network that drives B cell fate determination. Hence, we specifically chose *nfkb1*$^{-/-}$[46,52] and *IκBα*$^{SS/SS}$[53] (where *SS* denotes a model for Sjögren's syndrome) mouse strains as they alter the regulatory dynamics of the NF-κB signaling pathway. While the *nfkb1*$^{-/-}$ mice were previously reported to have substantially impaired antibody responses,[46,52] the *IκBα*$^{SS/SS}$ mutant has not yet been evaluated in this regard. We undertook *in vitro* dye dilution studies to measure cell fate decision proportions (death, division, plasma cell differentiation) across each generation of a proliferative burst (Figure 4A) and used these measurements to construct probabilistic cell fate maps for wild-type (WT), *nfkb1*$^{-/-}$, and *IκBα*$^{SS/SS}$ mice (Table 3, Figures S4A–S4D). Our measurements showed that compared with WT, *nfkb1*$^{-/-}$ mice have increased cell death but reduced plasma cell differentiation, whereas *IκBα*$^{SS/SS}$ mice show increases in both.

Model simulations using these measured cell fate maps, together with the physiologically relevant stochasticity and heritability parameter values (S = 16% and h = 95%, corresponding to the predicted theoretical optimum for S in Figure 2H and point of increase for h in Figure 3C and congruent with the experimental data fitted in Figure 3H), predicted higher total antibody titer for *IκBα*$^{SS/SS}$ mice and lower total antibody titer for *nfkb1*$^{-/-}$ mice, compared with WT (Figure 4B), consistent with their respectively higher or lower plasma cell differentiation rates (Figure S4D). We confirmed these predictions by comparing them against *in vivo* serum antibody titers in mice immunized with the model antigen 4-hydroxy-3-nitrophenylacetyl conjugated to chicken ovalbumin (NP_{21}-OVA), measured by using ELISA against NP_{25} to capture total NP-specific antibody (Figure 4C). The level of antibody produced by *nfkb1*$^{-/-}$ mice was too low to be reliably assessed and was thus not considered when analyzing affinities. Our simulations also predicted an unexpected decline in affinity maturation efficiency in *IκBα*$^{SS/SS}$ mice (Figure 4D). We confirmed this experimentally through diminished ratio of high-affinity (NP_5-binding) to total (NP_{25}-binding) antibodies in ELISA-based affinity ratio measurements (Figure 4E). On the other hand, simulations using measured cell fate maps but lacking either stochasticity (Figure 4F; S = 0 corresponding to deterministic clonal selection theory) or heritability (Figure 4G; S = 16%, h = 0 corresponding to the Cyton model) were unable to reproduce the *in vivo* observations.

To understand how the stochasticity and heritability of B cell fate decisions specify the relationship between *in vitro* B cell fate maps (Figure S4D) and the resulting *in vivo* titer and affinity of antibody output for each mutant strain, we systematically varied the S and h parameters and generated heatmaps for the speed of affinity maturation (Figure S4E), total antibody titer (Figure 4H), and high-affinity plasma cell fraction (Figure 4I). Consistent with our previous theoretical results, we found that some non-zero optimal stochasticity and increased heritability promote both the titer and speed of affinity maturation, and consequently the composite outcome of high-affinity plasma cell fraction, for all strains. Similarly, in each strain, we again found two distinct optima for titer and speed, which together determine the range where high-affinity plasma cell fraction is increased. The greater difference between the two optima in WT mice, where moderate S with high h accelerates affinity increase (Figure S4E top) but a greater S and lower h improve titer (Figure 4H left), results in a broader parameter range promoting high-affinity plasma cell formation (Figure 4I left). However, the increased differentiation rate in *IκBα*$^{SS/SS}$ mice (Figure S4D bottom) renders affinity maturation more sensitive to cell fate variability either preceding or during the proliferative burst, with a more stringent regime producing high-affinity plasma cells (Figure 4I right). While increased plasma differentiation in *IκBα*$^{SS/SS}$ mice intuitively results in high titers, their affinity maturation is generally slower due to removal of more high-affinity outliers, together diminishing the production of high-affinity plasma cells relative to WT at the physiologically relevant values of S = 16% and h = 95% (Figure 4E).

These results predict emergent properties of affinity maturation *in vivo*, parametrized only on the underlying distribution of B cell fate decisions measured *in vitro*. While the *in vitro* cell fate maps determine the potential range of cell fate outcomes for the B cell population within any evolutionary cycle, the stochasticity and heritability parameters specify the precise distribution of these cell fates, determining the evolutionary dynamics that produce emergent properties of the resulting antibodies.

Figure 5. Parameter sensitivity analysis predicts non-monotonic relationships between regulatory parameters within the GC and antibody response outcomes

(A–C) Line graphs showing how the speed of affinity gain (defined as the difference between median plasma cell affinities generated in the current and previous selection cycles) varies, with key cell biological parameters representing the rates of (A) cell death rate, (B) plasma cell differentiation rate, and (C) receptor mutation rate.

(D) Heatmap of the speed of affinity gain across the same differentiation-mutation parameter space.

(E and F) Heatmaps showing the total number of plasma cells generated above the high-affinity threshold (20.7 k_BT corresponding to K_D 1 nM),[33] during the (E) early or the (F) later phase of the GC response, as a function of the plasma cell differentiation rate and mutation rate.

(G) Schematic of simulations under the end-of-burst mutation model after each clonal burst.

(H and I) Line graphs showing (H) the speed of affinity gain and (I) the total number of high-affinity plasma cells under the end-of-burst mutation model. Points indicate the median across simulation runs, and shaded regions indicate the 95% confidence interval. Each parameter was varied in 1% increments, and each point represents the median of 2,000 Monte Carlo simulations.

(J) Speed of affinity gain of plasma cells at each cycle of affinity maturation across varying degrees of stochasticity in cell fate decisions, tested under three alternative assumptions about the distribution of BCR affinity changes (illustrated in red boxes above each plot). Left: narrow distribution; middle: broad distribution; right: uniform distribution. In all cases, the proportion of beneficial (affinity-enhancing) mutations is held constant, with affinity-enhancing mutations shaded, deleterious mutations shown as open bars, and neutral mutations in gray.

(K) Schematic of simulations across the stringency parameter K during selection that relaxes the hard threshold of the step function to a sigmoidal function.

(L and M) Heatmaps of (L) speed of affinity maturation and (M) total high-affinity plasma cell output across the space of selection stringency K and stochasticity parameter S. For all heatmaps, each parameter combination was evaluated using 2,000 Monte Carlo simulations to ensure statistical robustness.

See also Figure S5.

Please cite this article in press as: Xiang et al., Phased fragility and stability of non-genetic B cell states in the germinal center accelerate the genetic evolution of antibodies, Cell Systems (2026), https://doi.org/10.1016/j.cels.2026.101590

Table 1. List of all symbols and parameters used in the model equations

Symbol	Description	Value	Unit	Source
t	evolutionary cycle	1–40	–	based on Janeway et al.[18]
B	population of B cells	–	–	–
P	population of differentiated plasma cells	–	–	–
b	individual B cell	–	–	–
$\|B\|$	population size at each cycle	–	–	estimated for each cycle from Wittenbrink et al.[33]
$\|B\|_0$	population size of founder B cells at model initialization	50	–	estimated from Tas et al.[29]
A	distribution of B cell affinities	–	–	–
α_b	affinity of a B cell b	–	k_BT	–
$\overline{\alpha_0}$	mean affinity of founder B cells	11.4	k_BT	derived from estimated value of K_d = 10 μM[30]
σ_0	standard deviation of affinity among founder B cells	0.33	k_BT	assuming 99% of initial affinity distribution lies in the range of thermal fluctuation around α_0
α_{Th}	affinity threshold for selection	–	k_BT	estimated for each cycle from $\|B\|_{exp}(t)$
$F_b^0(\alpha)$	affinity-dependent fitness score of a cell b with affinity α	[0, 1]	–	–
F_b	redistributed fitness score of the cell b	[0, 1]	–	–
G	generation during clonal burst	[1, 8]	–	based on Gitlin et al.[42]
$\langle G \rangle$	average generation during clonal burst	3	–	based on Gitlin et al.[42]
ρ	Pearson correlation coefficient	[0, 1]	–	–
p_{Gi}	probability of terminating a clonal burst at i^{th} generation	–	–	–
S	stochasticity in cell fate decision	[0, 1]	–	–
σ_S	standard deviation in truncated normal function for distributing fitness score	–	–	estimated from S
h	non-genetic heritability in progeny	[0, 1]	–	–
$\Delta\alpha$	affinity change upon mutation	–	k_BT	–
p_m	probability of mutation in each division (Bernoulli trial)	0.5	–	derived from Kleinstein et al.,[43] and Kovaltsuk et al.[44]

Thus, incorporating the dynamic regulation of non-genetic variability is necessary to establish this robust alignment between knowledge-based mechanistic model predictions and experimental outcomes.

Computational acceleration for large-scale parameter sensitivity analysis

Building on the qualitative and quantitative agreement between our model predictions and experimental measurements, we next sought to systematically explore how individual mechanistic parameters shape emergent affinity maturation outcomes. This required a substantial expansion of the simulation space, both in the number of varied parameters and the in-depth Monte Carlo sampling needed to overcome the inherent probabilistic variation in clonal expansion and mutation. To enable this, we implemented an optimized simulation engine to yield a ~200× increase in computational throughput. This improvement allowed us to perform millions of independent simulations across densely sampled parameter grids, providing statistically stable estimates. The enhanced computational efficiency also allowed us to probe regions of parameter space that were previously inaccessible because of runtime limitations, thereby enabling the comprehensive sensitivity analysis presented below.

Affinity maturation as a function of B cell regulatory mechanisms

When underlying mechanisms are well captured, the strength of a mechanistic model lies in both its predictive power as well as its interpretability. To explain the observed relationships between B cell fate decisions and vaccine response outcomes, we used the model to explore how the relevant regulatory mechanisms impact affinity maturation. We looked at the cell death rate that removes low-affinity variants and plasma cell differentiation rate that removes high-affinity variants to produce plasma cells, which varied between our mutant strains. We further studied the effect of the mutation rate that controls the frequency at which these variants are generated.

We found that death rate alone has little impact on affinity gain (Figure 5A), plasma cell numbers, and affinities (Figures S5A and S5B). We attribute this to the exponential growth of high-affinity B cells over eight generations in a single GC cycle, rendering the system insensitive to the fate of lower-affinity cells. Extending this argument to memory B cells, which differentiate from lower

Table 2. Summary statistics for fitting stochasticity and heritability parameters

Parameter	Measurement	Value
Stochasticity	lineages terminating at division 0	34
	lineages terminating at division 1	29
	lineages terminating at division 2	27
	lineages terminating at division 3	89
	lineages terminating at division 4	66
	lineages terminating at division 5	108
	lineages terminating at division 6	8
	lineages terminating at division 7	1
	lineages terminating at division 8	1
Heritability	lineage sibling mismatch rate	0.09

affinity cells, we find that affinity gain and plasma cell numbers are unaffected. However, increasing this rate has clear benefits in improving clonal diversity of memory B cells (Figure S5C).

At the other end of the affinity range, increased plasma cell differentiation rates reduced speed of affinity gain (Figure 5B), as this removes high-affinity B cells from the Darwinian process. However, this also increases the number of effector plasma cells (Figure S5D). The balance results in a trade-off between titer and affinity as a function of differentiation rate, with optimal production of high-affinity plasma cells at moderate rates between 3% and 8% (Figure S5E). This explains why increased plasma cell differentiation produces a higher titer but lower affinity of antibodies in $I\kappa B\alpha^{SS/SS}$ mice compared with WT. Low-affinity B cells and thus memory B cell clonality remain unaffected (Figure S5F).

We further found that the mutation rate also showed an optimum between 0.3 and 0.5 mutations per daughter cell (Figure 5C). While a higher mutation rate generates more high-affinity variants, it also increases the risk of mutating away before they have had time to divide, and it produces more lethal mutations that reduce the number of progeny re-entering selection. Thus, optimal numbers of high-affinity plasma cells are generated when these processes are balanced at ~0.3 mutations per daughter cell (Figures S5G and S5H). The bias toward generating low-affinity variants also monotonically increases memory B cell clonality (Figure S5I).

We examined the combined effects of plasma cell differentiation and mutation rates on the speed of early (GC cycle 20) and late (GC cycle 40) high-affinity plasma cell counts (Figures 5D and 5E), as well as affinity gain (Figure 5F). Optimal conditions for high-affinity antibody production were stringent early on, peaking at 0.3 mutations per daughter cell and 2% plasma differentiation. However, after affinity maturation is established, more forgiving conditions allowed optimality across 0.1–0.4 mutations per daughter cell and 3%–12% differentiation rates. In contrast, total titer varied monotonically, similarly to when parameters were individually varied (Figures S5J and S5K). The speed of affinity gain landscape (Figure 5F) recapitulates the trends from one-dimensional parameter sweeps (Figures 5B and 5C) but now resolved across the full two-parameter space. These multidimensional results highlight that efficient affinity maturation requires a coordinated balance between sustaining GC residence, generating diversity, and avoiding mutational overload.

To evaluate whether our conclusions depended on the assumption that mutations occur continuously throughout a proliferative burst, we implemented an alternative "end-of-burst" mutation model in which daughter cells acquire mutations only after their final division event (Figure 5G). Despite this substantial change in underlying mechanistic assumptions, the qualitative behavior of the system remained unchanged. The speed of affinity gain (Figure 5H) exhibited the same characteristic peaked dependence on stochasticity observed earlier. Likewise, total high-affinity plasma cell output (Figure 5I) followed a parallel trend, showing the same non-monotonic dependence on stochasticity and preserving the relative ordering of outcomes. These results suggest that modifying the timing of mutation introduces only marginal effects on overall GC performance. Instead, the dominant factors shaping affinity maturation outcomes remain the degree of stochasticity and heritability in cell fate decisions.

To test whether our finding of an optimum stochasticity around 16% is sensitive to assumptions about the underlying distribution of antibody affinity changes upon mutation, we repeated the analysis using three alternative distributions with varied shapes but a fixed proportion of beneficial mutations (Figure 5J). Across all tested distributions, we consistently observed the same optimal range of stochasticity that maximized the speed of affinity gain. This supports the robustness of our conclusion that moderate stochasticity improves the efficiency of affinity maturation, independent of the exact shape of the affinity change distribution.

Finally, we relaxed the model's strict Darwinian selection assumption by replacing the hard affinity threshold, modeled as a step function, with imperfect selection where some low-affinity cells may escape death while high-affinity cells are eliminated, modeled as a sigmoidal function. This allowed us to systematically vary the stringency parameter (K) from 1 (perfectly affinity-dependent selection) to 0 (no affinity dependence) (Figure 5K). Under this softened selection regime, both the speed of affinity maturation (Figure 5L) and the total number of high-affinity plasma cells produced (Figure 5M) declined sharply as stringency decreased. Even modest relaxation of the threshold allowed lower-affinity clones—previously excluded from survival—to persist and proliferate, diluting the selective advantage of high-affinity variants. As a result, the efficiency of both affinity gain and high-affinity plasma cell output deteriorated markedly. These findings highlight that robust affinity maturation requires not only appropriate intracellular stochasticity and heritability (Figures 4 and 5) but also sufficiently stringent selection pressure to ensure that the fittest B cells disproportionately contribute to subsequent generations.

Overall, our findings from parameter sensitivity analyses provide intuition for the previously observed experimental outcomes for vaccine response differences between mouse strains and further predict that mutation and differentiation rates play important but non-monotonic roles in shaping affinity maturation dynamics through their impacts on high-affinity outliers. Further, the optimal rates for cell fate regulatory processes predicted by our model showed striking congruence with physiological estimates of ~0.5 mutations per cell[36,37] and 5% differentiation,[25,48] highlighting the reliability of the model as well as the fine-tuning of the GC for an effective plasma cell response.

Please cite this article in press as: Xiang et al., Phased fragility and stability of non-genetic B cell states in the germinal center accelerate the genetic evolution of antibodies, Cell Systems (2026), https://doi.org/10.1016/j.cels.2026.101590

Table 3. Table of cell fate decision threshold values quantified for different theoretical and experimentally derived cell fate maps

Parameter	Without PCs	With PCs	WT	nfkb1$^{-/-}$	IκBα$^{SS/SS}$
T_{X0}	0.0500	0.0500	0.1033	0.2550	0.0314
T_{X1}			0.0959	0.2907	0.0983
T_{X2}			0.1320	0.3001	0.3081
T_{X3}			0.1840	0.3351	0.5526
T_{X4}			0.2459	0.3978	0.6557
T_{X5}			0.3193	0.4589	0.6323
T_{X6}			0.3971	0.5140	0.5783
T_{X7}			0.4657	0.5190	0.5392
T_{X8}			0.6588	0.5947	0.7172
T_{R0}	0.0500	0.0500	0.1546	0.2883	0.0644
T_{R1}	0.1500	0.1400	0.2052	0.3689	0.1715
T_{R2}	0.5500	0.5300	0.3687	0.4260	0.3899
T_{R3}	0.8800	0.8600	0.5304	0.5335	0.6178
T_{R4}	0.9600	0.9200	0.6247	0.6458	0.7329
T_{R5}	0.9920	0.9380	0.6782	0.7154	0.7546
T_{R6}	0.9990	0.9460	0.7139	0.7577	0.7416
T_{R7}	0.9998	0.9495	0.7578	0.8086	0.7137
T_{R8}	1.0000	0.9500	0.9613	0.9952	0.8889
T_{P0}	–	0.9500	0.9674	0.9861	0.9902
T_{P1}			0.9443	0.9703	0.9854
T_{P2}			0.9615	0.9775	0.9756
T_{P3}			0.9762	0.9886	0.9583
T_{P4}			0.9758	0.9954	0.9363
T_{P5}			0.9680	0.9961	0.9034
T_{P6}			0.9566	0.9974	0.8747
T_{P7}			0.9505	0.9955	0.8576
T_{P8}			0.9613	0.9952	0.8889

DISCUSSION

Here, we report that the regulated fragility and stability of the non-genetic state of B cells have a critical role in determining the efficiency of generating high-affinity antibodies. Previous studies indicated that B cell non-genetic states are rendered fragile during stochastic sampling of selection signals in the LZ,[13] while they are stably maintained during rapid proliferative bursts in the DZ.[16] Scrambling the non-genetic state in the LZ allows some of the highest-affinity B cell clones to escape differentiation into plasma cells, fueling further rounds of affinity maturation. Conversely, the stable non-genetic cell state during proliferative bursts ensures maximum expansion of these high-affinity clones. Our insights clarify a key conflict in the literature—whether the seemingly stochastic B cell fate decision making[13–15] undermines the effectiveness of Darwinian genetic selection as described by classical clonal selection theory.[11]

Non-genetic variability in a population confers known evolutionary benefits[8] when leveraged for bet-hedging by diverse organisms including viruses,[54–56] bacteria,[57,58] yeast,[59] and mammalian tumor cells.[7,60] Heritability of non-genetic states was also shown to advantage genetic alleles in fluctuating environments,[61,62] while a lack of heritability can generate asymmetric cell fates during development.[63,64] In contrast, antibody affinity maturation is a developmental process involving selection of genetic variants for high affinity, but where affinity-defined fitness is not monotonic with the selected trait, as the highest-affinity cells terminate proliferation to become immune effector plasma cells.[65] These features define a unique role for non-genetic variability: to balance the need for effector formation while ensuring rapid affinity maturation, the GC reaction employs two alternating phases of non-genetic variability (fragility) and non-genetic heritability (stability). Further, the generation and maintenance of genetic and non-genetic variation is notably in anti-phase, as activation-induced cytidine deaminase (AID)-mediated mutation co-occurs with the proliferative burst in the DZ, while the non-genetic state is relatively stable, but not in the LZ during selection when the non-genetic state is affected by stochastic encounters with numerous cells and stimuli. This phase-structured coordination of genetic and non-genetic variation enables the GC to simultaneously optimize multiple, potentially competing, properties of the antibody response.

Our work also underscores the importance of genetic and non-genetic outliers rather than the average B cell in driving affinity maturation. Outlier cells and rare events dominate diverse immune processes from antiviral gene expression during infection[66] to selection within the GC itself[67–69]; hence, a predictive understanding must identify functionally relevant outliers and distinguish them from noise. This may challenge data-driven statistical inference methods that converge on a mean or dominant signal,[70,71] but it highlights a role for mechanistic models that can track relevant outliers. The present model formulation accounts for outliers along the singular dimension of fitness score combining affinity and non-genetic cell state. Future refinements could extend this framework to account for distinct molecular modules controlling survival, proliferation, and differentiation propensities—whose outlier distributions can interact in complex ways to shape affinity maturation.

The mechanistic model presented here reveals non-monotonic relationships between molecular regulatory parameters and affinity maturation, identifying optimal values that maximize antibody affinity gain or plasma cell production. These predicted optima align with physiological measurements in the literature (Figure 3H[25,36,37,48]), indicating that the process is finely tuned to maximize affinity gain, despite a wide parameter range where it remains robust but less efficient. Further, trade-offs are apparent among multiple aspects of the response, as improvements in speed come at the cost of plasma cell generation, and likewise between clonality and mutational depth. This suggests that a Pareto front is balancing the various properties of a vaccine response and that interventions for improvement should be targeting the goldilocks zone.

Although we formulated the mathematical model to gain fundamental insight into how non-genetic heterogeneity affects evolution of genetic antibody variants, our work suggests that the model also has forward predictive power, generating antibody response outcomes under molecular regulatory perturbations or for individuals with different genetic or health statuses. The mechanisms encoded in this knowledge-based model constrain its outputs and hence require far less training data for accurate prediction than purely data-driven models, with

the potential to extend these predictions beyond the training data. Notably, its interpretability allows identification of molecular targets for pharmacological perturbation and clinical translation. We suggest that clinical big data refinements of the mechanistic model may enable prediction of how small-molecule modifiers of signaling pathways can be used as adjuvants or co-treatments to improve outcomes in poorly responding patient cohorts to advance personalized vaccine administration.

Our findings are based on a mathematical model that incorporates a wealth of prior research in its underlying assumptions, structure, and parameter selection. The model's reliability is strengthened by sensitivity analyses, which revealed relationships aligned with expectation, measured rates of regulatory parameters, and perturbation studies using mutants to alter the regulatory network controlling B cell fate decisions. We specifically addressed variability in B cell fate decision-making in response to identical signals by abstracting the biological complexities of other GC processes. While other models have depicted stochastic interactions with antigen-presenting follicular dendritic cells and T follicular helper cells during B cell selection,[30,72] we reduced these to a dynamic affinity threshold consistent with current paradigms.[40] We also assumed perfect affinity-dependent selection to isolate the effect of cell fate variability, justified by the sequential and largely independent nature of the two processes. We disregarded epitope-specificity of B cell clones analogous to Brainbow-labeling studies of GC clonal dominance,[32] as well as mutation biases to assume uniform exploration of genetic variants. These strategic abstractions enabled us to focus on the fundamental question of how B cell non-genetic variability impacts affinity maturation.

While we found qualitative agreement between our model predictions and experimental observations of high-affinity antibody production in mouse strains with cell fate alterations, there was a quantitative discrepancy, with a drop of 13% in high-affinity antibody titer between WT and $I\kappa B\alpha^{SS/SS}$ predicted by the model but a more extreme effect of 40%, measured through serum ELISA. There are numerous potential reasons, such as (1) the definition of high-affinity antibody in simulations (total plasma cell counts with dissociation constant $[K_D] > 1$ nM) versus experiments (serum antibody fraction bound by NP_5 versus NP_{25} in ELISAs), (2) larger error estimates in experimental data compared with simulations, (3) the reliability of the *in vitro* experiments in determining cell fate decision maps that are relevant to *in vivo* conditions, (4) alterations in non-B cell processes relevant to the GC reaction, or (5) the reliability of the mathematical model itself. Nevertheless, the prediction of non-intuitive trends in emergent properties of the response, solely using *in vitro* measurements that were not used to train the model, highlights the promise of mechanistic modeling in enabling predictions across biological scales and human variations in the vaccine response.

RESOURCE AVAILABILITY

Lead contact

Further information and requests for resources and reagents should be directed to and will be fulfilled by the lead contact, Alexander Hoffmann (ahoffmann@ucla.edu).

Materials availability

This study did not generate new, unique materials.

Data and code availability

- Raw data (Flow Cytometry Standard (FCS) files, ELISA readouts) have been deposited at Zenodo. The DOIs for these data are listed in the key resources table.
- All modeling and analysis code has also been deposited at Zenodo, with the corresponding DOIs and repository URLs listed in the key resources table.
- Any additional information required to reanalyze the data reported in this paper is available from the lead contact upon request.

ACKNOWLEDGMENTS

We thank the members of the Hoffmann lab for valuable discussions and feedback on the manuscript, particularly Helen Huang, Chengyuan Li, Xiaolu Guo, Patrick Yuan, and Joseph Schirle as well as Roy Wollman and Eric Deeds for critical feedback and/or review of our manuscript. We acknowledge funding from NIH R01AI132731 and R01AI127867 to A.H., the JSMF and Damon Runyon Quantitative Biology (DRQ11-21) Postdoctoral Fellowships to H.V.N., and a UCLA Undergraduate Research Scholarship to V.K.

AUTHOR CONTRIBUTIONS

Conceptualization, A.H. and H.V.N.; methodology, M.Y.X. and H.V.N.; investigation, M.Y.X., H.V.N., V.K., R.V., and T.W.; visualization, M.Y.X.; writing – original draft, M.Y.X., H.V.N., and A.H.; writing – review and editing, M.Y.X., H.V.N., V.K., R.V., T.W., and A.H.; funding acquisition, A.H.; software, M.Y.X. and R.V.; and supervision, A.H.

DECLARATION OF INTERESTS

The authors declare no competing interests.

DECLARATION OF GENERATIVE AI AND AI-ASSISTED TECHNOLOGIES IN THE WRITING PROCESS

During the preparation of this work, the authors did not use any generative AI or AI-assisted technologies. The authors take full responsibility for the content of the publication.

STAR★METHODS

Detailed methods are provided in the online version of this paper and include the following:

- KEY RESOURCES TABLE
- EXPERIMENTAL MODEL AND STUDY PARTICIPANT DETAILS
  - Mice
  - Media and buffer compositions
  - B cell isolation
  - B cell in vitro culture
  - Measurement of generation-specific B-cell fate decisions by flow cytometry
  - Immunization and serum collection in live mice
  - Measurement of serum antibody by ELISA
- METHOD DETAILS
  - Defining the B cell population undergoing evolution
  - Initialization of the model by setting B cell population parameters
  - Selection operating upon the B cell population
  - Cell fate decisions and fitness in the subset of selected B cells
  - Stochasticity and non-genetic heritability of cell fate decisions
  - Mutation in the subset of dividing B cells
  - Modulating the stringency of affinity-dependent selection
  - Simulation details
- QUANTIFICATION AND STATISTICAL ANALYSIS
  - Fitting stochasticity and heritability parameters to experimental measurements
  - Flow cytometry analysis to generate cell fate maps

SUPPLEMENTAL INFORMATION

Supplemental information can be found online at https://doi.org/10.1016/j.cels.2026.101590.

Received: July 25, 2025
Revised: December 14, 2025
Accepted: March 24, 2026

REFERENCES

1. Avery, O.T., Macleod, C.M., and McCarty, M. (1944). Studies on the chemical nature of the substance inducing transformation of pneumococcal types: induction of transformation by a desoxyribonucleic acid fraction isolated from pneumococcus type III. J. Exp. Med. *79*, 137–158. https://doi.org/10.1084/jem.79.2.137.
2. Waddington, C.H. (2012). The epigenotype. 1942. Int. J. Epidemiol. *41*, 10–13. https://doi.org/10.1093/ije/dyr184.
3. Waddington, C.H. (1957). The Strategy of the Genes: A Discussion of Some Aspects of Theoretical Biology (Allen & Unwin).
4. Zhang, B., Srivastava, A., Mimitou, E., Stuart, T., Raimondi, I., Hao, Y., Smibert, P., and Satija, R. (2022). Characterizing cellular heterogeneity in chromatin state with scCUT&Tag-pro. Nat. Biotechnol. *40*, 1220–1230. https://doi.org/10.1038/s41587-022-01250-0.
5. Cha, J., and Lee, I. (2020). Single-cell network biology for resolving cellular heterogeneity in human diseases. Exp. Mol. Med. *52*, 1798–1808. https://doi.org/10.1038/s12276-020-00528-0.
6. Mattiazzi Usaj, M., Yeung, C.H.L., Friesen, H., Boone, C., and Andrews, B. J. (2021). Single-cell image analysis to explore cell-to-cell heterogeneity in isogenic populations. Cell Syst. *12*, 608–621. https://doi.org/10.1016/j.cels.2021.05.010.
7. Spencer, S.L., Gaudet, S., Albeck, J.G., Burke, J.M., and Sorger, P.K. (2009). Non-genetic origins of cell-to-cell variability in TRAIL-induced apoptosis. Nature *459*, 428–432. https://doi.org/10.1038/nature08012.
8. Balázsi, G., van Oudenaarden, A., and Collins, J.J. (2011). Cellular decision making and biological noise: from microbes to mammals. Cell *144*, 910–925. https://doi.org/10.1016/j.cell.2011.01.030.
9. Cheong, R., Rhee, A., Wang, C.J., Nemenman, I., and Levchenko, A. (2011). Information transduction capacity of noisy biochemical signaling networks. Science *334*, 354–358. https://doi.org/10.1126/science.1204553.
10. Adelaja, A., Taylor, B., Sheu, K.M., Liu, Y., Luecke, S., and Hoffmann, A. (2021). Six distinct NFκB signaling codons convey discrete information to distinguish stimuli and enable appropriate macrophage responses. Immunity *54*, 916–930.e7. https://doi.org/10.1016/j.immuni.2021.04.011.
11. Burnet, F.M. (1959). The Clonal Selection Theory of Acquired Immunity (Vanderbilt University Press). https://doi.org/10.5962/bhl.title.8281.
12. Lyons, A.B., and Parish, C.R. (1994). Determination of lymphocyte division by flow cytometry. J. Immunol. Methods *171*, 131–137. https://doi.org/10.1016/0022-1759(94)90236-4.
13. Hawkins, E.D., Turner, M.L., Dowling, M.R., van Gend, C., and Hodgkin, P. D. (2007). A model of immune regulation as a consequence of randomized lymphocyte division and death times. Proc. Natl. Acad. Sci. USA *104*, 5032–5037. https://doi.org/10.1073/pnas.0700026104.
14. Hawkins, E.D., Markham, J.F., McGuinness, L.P., and Hodgkin, P.D. (2009). A single-cell pedigree analysis of alternative stochastic lymphocyte fates. Proc. Natl. Acad. Sci. USA *106*, 13457–13462. https://doi.org/10.1073/pnas.0905629106.
15. Duffy, K.R., Wellard, C.J., Markham, J.F., Zhou, J.H.S., Holmberg, R., Hawkins, E.D., Hasbold, J., Dowling, M.R., and Hodgkin, P.D. (2012). Activation-induced B cell fates are selected by intracellular stochastic competition. Science *335*, 338–341. https://doi.org/10.1126/science.1213230.
16. Mitchell, S., Roy, K., Zangle, T.A., and Hoffmann, A. (2018). Nongenetic origins of cell-to-cell variability in B lymphocyte proliferation. Proc. Natl. Acad. Sci. USA *115*, E2888–E2897. https://doi.org/10.1073/pnas.1715639115.
17. Mesin, L., Ersching, J., and Victora, G.D. (2016). Germinal center B cell dynamics. Immunity *45*, 471–482. https://doi.org/10.1016/j.immuni.2016.09.001.
18. Janeway, C.A., J., Travers, P., Walport, M., and Shlomchik, M.J. (2001). The course of the adaptive response to infection. In Immunobiology: the Immune System in Health and Disease, Fifth Edition (Garland Science).
19. Shlomchik, M.J., and Weisel, F. (2012). Germinal center selection and the development of memory B and plasma cells. Immunol. Rev. *247*, 52–63. https://doi.org/10.1111/j.1600-065X.2012.01124.x.
20. Pae, J., Schwan, N., Ottino-Loffler, B., DeWitt, W.S., Garg, A., Bortolatto, J., Vora, A.A., Shen, J.-J., Hobbs, A., Castro, T.B.R., et al. (2025). Transient silencing of hypermutation preserves B cell affinity during clonal bursting. Nature *641*, 486–494. https://doi.org/10.1038/s41586-025-08687-8.
21. Kennedy, D.E., Okoreeh, M.K., Maienschein-Cline, M., Ai, J., Veselits, M., McLean, K.C., Dhungana, Y., Wang, H., Peng, J., Chi, H., et al. (2020). Novel specialized cell state and spatial compartments within the germinal center. Nat. Immunol. *21*, 660–670. https://doi.org/10.1038/s41590-020-0660-2.
22. King, H.W., Wells, K.L., Shipony, Z., Kathiria, A.S., Wagar, L.E., Lareau, C., Orban, N., Capasso, R., Davis, M.M., Steinmetz, L.M., et al. (2021). Integrated single-cell transcriptomics and epigenomics reveals strong germinal center-associated etiology of autoimmune risk loci. Sci. Immunol. *6*, eabh3768. https://doi.org/10.1126/sciimmunol.abh3768.
23. Iber, D., and Maini, P.K. (2002). A mathematical model for germinal centre kinetics and affinity maturation. J. Theor. Biol. *219*, 153–175. https://doi.org/10.1006/jtbi.2002.3079.
24. Kepler, T.B. (2013). Reconstructing a B-cell clonal lineage. I. Statistical inference of unobserved ancestors. F1000Res *2*, 103. https://doi.org/10.12688/f1000research.2-103.v1.
25. Weisel, F.J., Zuccarino-Catania, G.V., Chikina, M., and Shlomchik, M.J. (2016). A Temporal Switch in the Germinal Center Determines Differential Output of Memory B and Plasma Cells. Immunity *44*, 116–130. https://doi.org/10.1016/j.immuni.2015.12.004.
26. Thomas, M.J., Klein, U., Lygeros, J., and Rodríguez Martínez, M. (2019). A Probabilistic Model of the Germinal Center Reaction. Front. Immunol. *10*, 689. https://doi.org/10.3389/fimmu.2019.00689.
27. Pélissier, A., Akrout, Y., Jahn, K., Kuipers, J., Klein, U., Beerenwinkel, N., and Rodríguez Martínez, M. (2020). Computational Model Reveals a Stochastic Mechanism behind Germinal Center Clonal Bursts. Cells *9*, 1448. https://doi.org/10.3390/cells9061448.
28. Seyrek, K., Ivanisenko, N.V., Wohlfromm, F., Espe, J., and Lavrik, I.N. (2021). Impact of human CD95 mutations on cell death and autoimmunity: a model. Trends Immunol. *43*, 22–40. https://doi.org/10.1016/j.it.2021.11.006.
29. Van Beek, M., Nussenzweig, M.C., and Chakraborty, A.K. (2022). Two complementary features of humoral immune memory confer protection against the same or variant antigens. Proc. Natl. Acad. Sci. USA *119*, e2205598119. https://doi.org/10.1073/pnas.2205598119.
30. Merino Tejero, E., Lashgari, D., García-Valiente, R., Gao, X., Crauste, F., Robert, P.A., Meyer-Hermann, M., Martínez, M.R., van Ham, S.M., Guikema, J.E.J., et al. (2021). Multiscale Modeling of Germinal Center Recapitulates the Temporal Transition From Memory B Cells to Plasma Cells Differentiation as Regulated by Antigen Affinity-Based Tfh Cell Help. Front. Immunol. *11*, 620716. https://doi.org/10.3389/fimmu.2020.620716.
31. Mu, D.P., Scharer, C.D., Kaminski, N.E., and Zhang, Q. (2024). A multiscale spatial modeling framework for the germinal center response. Front. Immunol. *15*, 1377303. https://doi.org/10.3389/fimmu.2024.1377303.
32. Tas, J.M.J., Mesin, L., Pasqual, G., Targ, S., Jacobsen, J.T., Mano, Y.M., Chen, C.S., Weill, J.-C., Reynaud, C.-A., Browne, E.P., et al. (2016). Visualizing antibody affinity maturation in germinal centers. Science *351*, 1048–1054. https://doi.org/10.1126/science.aad3439.

33. Eisen, H.N. (2014). Affinity Enhancement of Antibodies: How Low-Affinity Antibodies Produced Early in Immune Responses Are Followed by High-Affinity Antibodies Later and in Memory B-Cell Responses. Cancer Immunol. Res. *2*, 381–392. https://doi.org/10.1158/2326-6066.CIR-14-0029.

34. Wittenbrink, N., Klein, A., Weiser, A.A., Schuchhardt, J., and Or-Guil, M. (2011). Is There a Typical Germinal Center? A Large-Scale Immunohistological Study on the Cellular Composition of Germinal Centers during the Hapten-Carrier–Driven Primary Immune Response in Mice. J. Immunol. *187*, 6185–6196. https://doi.org/10.4049/jimmunol.1101440.

35. Victora, G.D., and Nussenzweig, M.C. (2022). Germinal Centers. Annu. Rev. Immunol. *40*, 413–442. https://doi.org/10.1146/annurev-immunol-120419-022408.

36. Kleinstein, S.H., Louzoun, Y., and Shlomchik, M.J. (2003). Estimating hypermutation rates from clonal tree data. J. Immunol. *171*, 4639–4649. https://doi.org/10.4049/jimmunol.171.9.4639.

37. Kovaltsuk, A., Krawczyk, K., Galson, J.D., Kelly, D.F., Deane, C.M., and Trück, J. (2017). How B-Cell Receptor Repertoire Sequencing Can Be Enriched with Structural Antibody Data. Front. Immunol. *8*, 1753. https://doi.org/10.3389/fimmu.2017.01753.

38. Shannon, M., and Mehr, R. (1999). Reconciling repertoire shift with affinity maturation: the role of deleterious mutations. J. Immunol. *162*, 3950–3956. https://doi.org/10.4049/jimmunol.162.7.3950.

39. Zhang, J., and Shakhnovich, E.I. (2010). Optimality of mutation and selection in germinal centers. PLoS Comput. Biol. *6*, e1000800. https://doi.org/10.1371/journal.pcbi.1000800.

40. Schwickert, T.A., Victora, G.D., Fooksman, D.R., Kamphorst, A.O., Mugnier, M.R., Gitlin, A.D., Dustin, M.L., and Nussenzweig, M.C. (2011). A dynamic T cell-limited checkpoint regulates affinity-dependent B cell entry into the germinal center. J. Exp. Med. *208*, 1243–1252. https://doi.org/10.1084/jem.20102477.

41. Shih, T.-A.Y., Meffre, E., Roederer, M., and Nussenzweig, M.C. (2002). Role of BCR affinity in T cell dependent antibody responses in vivo. Nat. Immunol. *3*, 570–575. https://doi.org/10.1038/ni803.

42. Merino Tejero, E., Mao, Q., Lashgari, D., García-Valiente, R., Robert, P.A., Meyer-Hermann, M., Rodríguez Martínez, M., Guikema, J.E.J., Hoefsloot, H.H.C., and van Kampen, A.H.C. (2022). Multi-Scale Modeling Recapitulates the Effect of Genetic Alterations Associated With Diffuse Large B-Cell Lymphoma in the Germinal Center Dynamics. Front. Syst. Biol. *2*, 864690. https://doi.org/10.3389/fsysb.2022.864690.

43. Burnet, F.M. (1976). A modification of Jerne's theory of antibody production using the concept of clonal selection. CA Cancer J. Clin. *26*, 119–121. https://doi.org/10.3322/canjclin.26.2.119.

44. Mayer, C.T., Gazumyan, A., Kara, E.E., Gitlin, A.D., Golijanin, J., Viant, C., Pai, J., Oliveira, T.Y., Wang, Q., Escolano, A., et al. (2017). The microanatomic segregation of selection by apoptosis in the germinal center. Science *358*, eaao2602. https://doi.org/10.1126/science.aao2602.

45. Gitlin, A.D., Shulman, Z., and Nussenzweig, M.C. (2014). Clonal selection in the germinal centre by regulated proliferation and hypermutation. Nature *509*, 637–640. https://doi.org/10.1038/nature13300.

46. Shokhirev, M.N., and Hoffmann, A. (2013). FlowMax: A Computational Tool for Maximum Likelihood Deconvolution of CFSE Time Courses. PLoS One *8*, e67620. https://doi.org/10.1371/journal.pone.0067620.

47. Inoue, T., Moran, I., Shinnakasu, R., Phan, T.G., and Kurosaki, T. (2018). Generation of memory B cells and their reactivation. Immunol. Rev. *283*, 138–149. https://doi.org/10.1111/imr.12640.

48. Scharer, C.D., Patterson, D.G., Mi, T., Price, M.J., Hicks, S.L., and Boss, J.M. (2020). Antibody-secreting cell destiny emerges during the initial stages of B-cell activation. Nat. Commun. *11*, 3989. https://doi.org/10.1038/s41467-020-17798-x.

49. Shinnakasu, R., Inoue, T., Kometani, K., Moriyama, S., Adachi, Y., Nakayama, M., Takahashi, Y., Fukuyama, H., Okada, T., and Kurosaki, T. (2016). Regulated selection of germinal-center cells into the memory B cell compartment. Nat. Immunol. *17*, 861–869. https://doi.org/10.1038/ni.3460.

50. Viant, C., Weymar, G.H.J., Escolano, A., Chen, S., Hartweger, H., Cipolla, M., Gazumyan, A., and Nussenzweig, M.C. (2020). Antibody Affinity Shapes the Choice between Memory and Germinal Center B Cell Fates. Cell *183*, 1298–1311.e11. https://doi.org/10.1016/j.cell.2020.09.063.

51. Wong, R., Belk, J.A., Govero, J., Uhrlaub, J.L., Reinartz, D., Zhao, H., Errico, J.M., D'Souza, L., Ripperger, T.J., Nikolich-Zugich, J., et al. (2020). Affinity-Restricted Memory B Cells Dominate Recall Responses to Heterologous Flaviviruses. Immunity *53*, 1078–1094.e7. https://doi.org/10.1016/j.immuni.2020.09.001.

52. Sha, W.C., Liou, H.C., Tuomanen, E.I., and Baltimore, D. (1995). Targeted disruption of the p50 subunit of NF-kappa B leads to multifocal defects in immune responses. Cell *80*, 321–330. https://doi.org/10.1016/0092-8674(95)90415-8.

53. Peng, B., Ling, J., Lee, A.J., Wang, Z., Chang, Z., Jin, W., Kang, Y., Zhang, R., Shim, D., Wang, H., et al. (2010). Defective feedback regulation of NF-kappaB underlies Sjogren's syndrome in mice with mutated kappaB enhancers of the IkappaBalpha promoter. Proc. Natl. Acad. Sci. USA *107*, 15193–15198. https://doi.org/10.1073/pnas.1005533107.

54. Arkin, A., Ross, J., and McAdams, H.H. (1998). Stochastic kinetic analysis of developmental pathway bifurcation in phage lambda-infected Escherichia coli cells. Genetics *149*, 1633–1648. https://doi.org/10.1093/genetics/149.4.1633.

55. Ptashne, M. (2004). A Genetic Switch: Phage Lambda Revisited (Cold Spring Harbor Laboratory Press).

56. Weinberger, L.S., Burnett, J.C., Toettcher, J.E., Arkin, A.P., and Schaffer, D.V. (2005). Stochastic gene expression in a lentiviral positive-feedback loop: HIV-1 Tat fluctuations drive phenotypic diversity. Cell *122*, 169–182. https://doi.org/10.1016/j.cell.2005.06.006.

57. Balaban, N.Q., Merrin, J., Chait, R., Kowalik, L., and Leibler, S. (2004). Bacterial persistence as a phenotypic switch. Science *305*, 1622–1625. https://doi.org/10.1126/science.1099390.

58. Maamar, H., Raj, A., and Dubnau, D. (2007). Noise in gene expression determines cell fate in Bacillus subtilis. Science *317*, 526–529. https://doi.org/10.1126/science.1140818.

59. Acar, M., Becskei, A., and van Oudenaarden, A. (2005). Enhancement of cellular memory by reducing stochastic transitions. Nature *435*, 228–232. https://doi.org/10.1038/nature03524.

60. Jia, D., Jolly, M.K., Kulkarni, P., and Levine, H. (2017). Phenotypic Plasticity and Cell Fate Decisions in Cancer: Insights from Dynamical Systems Theory. Cancers *9*, 70. https://doi.org/10.3390/cancers9070070.

61. Jablonka, E., and Raz, G. (2009). Transgenerational epigenetic inheritance: prevalence, mechanisms, and implications for the study of heredity and evolution. Q. Rev. Biol. *84*, 131–176. https://doi.org/10.1086/598822.

62. Carja, O., and Plotkin, J.B. (2019). Evolutionary Rescue Through Partly Heritable Phenotypic Variability. Genetics *211*, 977–988. https://doi.org/10.1534/genetics.118.301758.

63. Chang, H.H., Hemberg, M., Barahona, M., Ingber, D.E., and Huang, S. (2008). Transcriptome-wide noise controls lineage choice in mammalian progenitor cells. Nature *453*, 544–547. https://doi.org/10.1038/nature06965.

64. Abadie, K., Clark, E.C., Valanparambil, R.M., Ukogu, O., Yang, W., Daza, R.M., Ng, K.K.H., Fathima, J., Wang, A.L., Lee, J., et al. (2024). Reversible, tunable epigenetic silencing of TCF1 generates flexibility in the T cell memory decision. Immunity *57*, 271–286.e13. https://doi.org/10.1016/j.immuni.2023.12.006.

65. Shapiro-Shelef, M., and Calame, K. (2005). Regulation of plasma-cell development. Nat. Rev. Immunol. *5*, 230–242. https://doi.org/10.1038/nri1572.

66. Shalek, A.K., Satija, R., Shuga, J., Trombetta, J.J., Gennert, D., Lu, D., Chen, P., Gertner, R.S., Gaublomme, J.T., Yosef, N., et al. (2014). Single-cell RNA-seq reveals dynamic paracrine control of cellular variation. Nature *510*, 363–369. https://doi.org/10.1038/nature13437.

67. Allen, C.D.C., Okada, T., and Cyster, J.G. (2007). Germinal-center organization and cellular dynamics. Immunity *27*, 190–202. https://doi.org/10.1016/j.immuni.2007.07.009.

68. Shulman, Z., Gitlin, A.D., Weinstein, J.S., Lainez, B., Esplugues, E., Flavell, R.A., Craft, J.E., and Nussenzweig, M.C. (2014). Dynamic signaling by T follicular helper cells during germinal center B cell selection. Science *345*, 1058–1062. https://doi.org/10.1126/science.1257861.

69. Young, C., and Brink, R. (2021). The unique biology of germinal center B cells. Immunity *54*, 1652–1664. https://doi.org/10.1016/j.immuni.2021.07.015.

70. Tsang, J.S., Schwartzberg, P.L., Kotliarov, Y., Biancotto, A., Xie, Z., Germain, R.N., Wang, E., Olnes, M.J., Narayanan, M., Golding, H., et al. (2014). Global analyses of human immune variation reveal baseline predictors of postvaccination responses. Cell *157*, 499–513. https://doi.org/10.1016/j.cell.2014.03.031.

71. Fourati, S., Tomalin, L.E., Mulè, M.P., Chawla, D.G., Gerritsen, B., Rychkov, D., Henrich, E., Miller, H.E.R., Hagan, T., Diray-Arce, J., et al. (2022). Pan-vaccine analysis reveals innate immune endotypes predictive of antibody responses to vaccination. Nat. Immunol. *23*, 1777–1787. https://doi.org/10.1038/s41590-022-01329-5.

72. Meyer-Hermann, M., Mohr, E., Pelletier, N., Zhang, Y., Victora, G.D., and Toellner, K.-M. (2012). A Theory of Germinal Center B Cell Selection, Division, and Exit. Cell Rep. *2*, 162–174. https://doi.org/10.1016/j.celrep.2012.05.010.

73. Nojima, T., Haniuda, K., Moutai, T., Matsudaira, M., Mizokawa, S., Shiratori, I., Azuma, T., and Kitamura, D. (2011). In-vitro derived germinal centre B cells differentially generate memory B or plasma cells in vivo. Nat. Commun. *2*, 465. https://doi.org/10.1038/ncomms1475.

74. Victora, G.D., and Nussenzweig, M.C. (2012). Germinal centers. Annu. Rev. Immunol. *30*, 429–457. https://doi.org/10.1146/annurev-immunol-020711-075032.

75. Victora, G.D., Schwickert, T.A., Fooksman, D.R., Kamphorst, A.O., Meyer-Hermann, M., Dustin, M.L., and Nussenzweig, M.C. (2010). Germinal center dynamics revealed by multiphoton microscopy with a photoactivatable fluorescent reporter. Cell *143*, 592–605. https://doi.org/10.1016/j.cell.2010.10.032.

Please cite this article in press as: Xiang et al., Phased fragility and stability of non-genetic B cell states in the germinal center accelerate the genetic evolution of antibodies, Cell Systems (2026), https://doi.org/10.1016/j.cels.2026.101590

STAR★METHODS

KEY RESOURCES TABLE

REAGENT or RESOURCE	SOURCE	IDENTIFIER
Antibodies		
Rat monoclonal anti-human/ mouse B220-APC	Biolegend	103212; RRID: AB_312997
Rat monoclonal anti-mouse CD138-PE (Clone 281-2)	Biolegend	142504; RRID: AB_10916119
Recombinant mouse monoclonal anti-NP [B1-8] standard 1mg/mL	Abcam	ab206535
Goat anti-mouse polyclonal IgG-biotin	Abcam	ab6788; RRID: AB_954885
Chemicals, peptides, and recombinant proteins		
RPMI	Gibco	11875-093
CpG (ODN1668)	Invivogen	tlrl-1668-1
CD154 (CD40 ligand)	Biolegend	797406
Murine recombinant BAFF/BlyS/TNFSF13B	R&D Systems	2106-BF-010
Murine recombinant IL-4	PeproTech	214-14
Murine recombinant IL-21	PeproTech	210-21
NP_{21}-OVA	Biosearch Technologies	N-5051-10
NP_{21-29}-CGG	Santa Cruz Biotechnologies	sc-396209
NP_{1-9}-CGG	Santa Cruz Biotechnologies	sc-396187
Alhydrogel	Invivogen	vac-alu-250
Critical commercial assays		
CellTrace™ Far Red Proliferation Kit	ThermoFisher Scientific	C34564
Streptavidin-HRP	R&D Systems	DY998
TMB color reagent for ELISA	R&D Systems	DY999B
Deposited Data		
ELISA	This Study	Zenodo: 10.5281/zenodo.18778833
FLOW	This Study	Zenodo: 10.5281/zenodo.18778833
Experimental models: Cell lines		
NIH 3T3 cells	ATCC	CRL-1658
Experimental models: Organisms/strains		
Mouse: C57BL/6	The Jackson Laboratory	JAX: 000664; RRID: IMSR_JAX:000664
Mouse: C57BL/6: *nfkb1*$^{-/-}$	The Jackson Laboratory	JAX: 006097; RRID: IMSR_JAX:006097
Mouse: C57BL/6: $I\kappa B\alpha^{SS/SS}$	The Jackson Laboratory	RRID: IMSR_JAX:037800
Software and algorithms		
FlowJO V10.4.2	FlowJO LLC	N/A
Python v3.7.164-bit base: Conda	Anaconda v3.0	N/A
Original simulation and analysis code	This Study	Zenodo: 10.5281/zenodo.18778833; GitHub: https://github.com/signalingsystemslab/GC_evolution_model
High-performance simulation code	This Study	Zenodo: 10.5281/zenodo.18807521; Github: https://github.com/signalingsystemslab/gc-model

Please cite this article in press as: Xiang et al., Phased fragility and stability of non-genetic B cell states in the germinal center accelerate the genetic evolution of antibodies, Cell Systems (2026), https://doi.org/10.1016/j.cels.2026.101590

EXPERIMENTAL MODEL AND STUDY PARTICIPANT DETAILS

Mice

Mice were maintained in environmental control facilities at the University of California, Los Angeles. Biological replicates were typically neither age- nor sex-matched, were not littermates, and often not co-housed, in order to determine whether differences between genotypes were indeed greater than differences between individuals within the same genotype. All mice used in experiments were 8-20 weeks old. The wild-type, *nfkb1*$^{-/-}$[46,52] and IκB$\alpha^{SS/SS}$[10,53] mice were all on the C57BL/6 genetic background. Animal work was performed according to University of California, Los Angeles regulations under approved protocols.

Media and buffer compositions

B cell media

RPMI 1650 (Gibco) supplemented with 100 IU Penicillin, 100 μg/ml Streptomycin, 5 mM L-glutamine, 20 mM HEPES buffer, 1mM MEM non-essential amino acids, 1 mM sodium pyruvate, 10% fetal bovine serum (FBS), and 55 μM 2-Mercaptoethanol.

MACS buffer

Phosphate buffered saline (pH 7.4), 2% FBS, 100 IU Penicillin, 100 μg/ml Streptomycin.

ELISA coating buffer

Phosphate buffered saline (pH 7.4).

ELISA sample dilution buffer

Phosphate buffered saline (pH 7.4), 0.1% bovine serum albumin (BSA), 0.025% Tween-20.

ELISA blocking buffer

Phosphate buffered saline (pH 7.4), 1% BSA.

ELISA wash buffer

Phosphate buffered saline (pH 7.4), 0.1% BSA, 0.5% Tween-20.

B cell isolation

Spleens were harvested from 8 to 20-week-old male and female C57BL/6 wild type, *nfkb1*$^{-/-}$, and IκB$\alpha^{SS/SS}$ mice. For negative selection of B cells, homogenized splenocytes were incubated with anti-CD43 magnetic beads for 15 min at 4-8 °C, washed with MACS buffer and passed through an LS column (Miltenyi Biotech). The purity of B cells was assessed at >98% based on B220 staining as described previously.[16] Follicular B cells were then further purified from the enriched B cell population by positive selection, by labeling with anti-CD23 microbeads (Miltenyi Biotech) for 15 min at 4-8°C, followed by washing with MACS buffer and elution from an LS column. The purity of follicular B cells was assessed at >99% using B220^{+} CD21^{mid} CD23^{hi} staining, distinguished from marginal zone (B220^{+} CD21^{hi} CD23^{lo}) B cells by flow cytometry.

B cell in vitro culture

We developed a B cell co-culture system to mimic germinal center follicles as closely as possible, based on prior work,[73] while still retaining control over the quantity of various stimuli available to each B cell. Briefly, NIH 3T3 fibroblasts were used to mimic the presence of stromal cells providing mechanical cues to B cells, plated at a starting density of 10,000 per well in the 48-well plate and allowed to adhere for ~8 hours prior to seeding follicular B cells. Pure follicular B cells were seeded at a density of 100,000 starting cells per well in a 48-well plate and cultured for 6 days in fresh RPMI-based media at 37 °C and 5% CO_2. Cells were stimulated with 50 ng/mL BAFF in solution to maintain survival. T-dependent stimuli were mimicked by adding 100 ng/mL CD154 (CD40 ligand) as a soluble peptide fragment, along with the cytokines 2 ng/mL IL-4 to promote proliferation and 1 ng/mL IL-21 to promote plasma differentiation. We determined these by first evaluating a range of doses for each stimulus to identify their lower non-responding and upper saturating doses, choosing their geometric mean as the representative dose in culture. B cells were harvested at 120 hours to quantify proportions of various cell fates by flow cytometry.

Measurement of generation-specific B-cell fate decisions by flow cytometry

Immediately following isolation and prior to culture, WT, *nfkb1*$^{-/-}$ and IκB$\alpha^{SS/SS}$ B cells were stained with Cell Trace Far Red (CTFR) using the CellTrace Far Red Cell Proliferation Kit (ThermoFisher Scientific, # C34564) as described by the manufacturer protocol. Briefly, 2M cells were resuspended in 1 mL RT PBS and incubated with 1 μL CTFR for 25 min at RT with rotation. Cells were washed by centrifuging, resuspending in 1 mL RPMI with 10% FBS, and incubating until continuous mixing for 10 min at RT. The washing steps were repeated a total of 3 times. CTFR labeled cells were cultured for 120 hrs as described above. B cells were harvested by pipetting gently to resuspend them in the culture media without detaching the adherent 3T3 cells, collecting them in the supernatant, washing in PBS, and staining with 1:1000 anti-CD138-PE diluted in PBS with 15 minutes incubation for plasma cell identification. Samples were acquired on the CytoFlex flow cytometer (CytoFlex, Beckman Coulter). The cells were gated based on forward scatter (FSC) and side scatter (SSC) to identify live single cells. Doublets were excluded from the analysis using FSC area and height. Cell generation numbers were defined based on dilution of CTFR, and plasma cells identified as CD138^{hi}. Further quantitative analyses to estimate cell numbers per generation undergoing each fate were performed as described below.

Immunization and serum collection in live mice

Mice were immunized with the model antigen NP_{21}-OVA (Biosearch Technologies) adsorbed on the adjuvant Alhydrogel 2% (Invivogen). A 5 mg/mL stock of NP_{21}-OVA and 10% Alhydrogel were mixed in a 1:1 volumetric ratio by pipetting vigorously for 10 minutes. 8- to 20-week-old male and female C57BL/6 wild type, *nfkb1*$^{-/-}$, and IκB$\alpha^{SS/SS}$ mice were immunized subcutaneously in the left hind footpad with 30 μL of the mixture using 31G insulin syringes, corresponding to 30 μg NP_{21}-OVA and 60μg adjuvant for each mouse as per established protocols.[74] Only a single priming dose was administered to monitor affinity maturation, as the computational model does not explicitly account for recruitment of memory cells in a boosted response. About 50 μL blood was collected retro-orbitally from each mouse in non-heparinized glass capillaries at 0-, 5-, 8-, 11-, 15-, and 18-days post immunization, alternating between left and right eyes to minimize injury. Blood samples were placed at room temperature for at least 3 hours to initiate clotting, maintained overnight at 4 °C, centrifuged at 500 rcf for 5 minutes to separate clot from serum with minimum hemolysis, after which about 20 μL supernatant serum was collected. Centrifugation and supernatant collection were repeated to fully remove all debris, and purified serum samples were stored at -20 °C until antibody content was assessed by ELISA.

Measurement of serum antibody by ELISA

ELISA protocols were adapted from established protocols (R&D Systems). Total antibody quantity was estimated by binding against NP_{25} oligomers and high-affinity fraction by binding against NP_5 oligomers, with both oligomers conjugated to chicken gamma globulin (CGG) as a neutral carrier distinct from the conjugate immunogen ovalbumin (OVA). ELISA plates were prepared for capture by coating with 1 μg/mL capture reagent (NP_{21-29}-CGG or NP_{1-9}-CGG, Santa Cruz Biotechnologies) diluted in PBS. 50 μL coating reagent was applied to each well of a 96-well half-area plate and incubated overnight at 4 °C. Coated plates were washed according to a standard wash protocol of 3 times in ELISA wash buffer with 3 minutes of shaking each time, once more without shaking, and finally once in distilled water to remove excess coating reagent. All subsequent incubations were done at room temperature with continuous shaking for 1 hour unless specified otherwise. Plates were blocked in 200 μL ELISA blocking buffer before washing. Samples were diluted to concentrations between 1:10,000 and 1:100,000 in ELISA sample dilution buffer, 50 μL each applied to sample wells and incubated. Recombinant monoclonal B1-8 antibody (1 mg/mL stock) with known high affinity against NP was used to prepare standards at five serial dilutions between 1 μg/mL and 1 ng/mL, with anti-tubulin as a negative control, and ELISA sample dilution buffer as blanks. Samples were washed off and incubated with 50 μL/well detection antibody (goat anti-mouse IgG-biotin) diluted to a working concentration of 0.5 μg/mL in ELISA sample diluent buffer. After washing again, plates were incubated for 20 minutes with 10 μg/mL streptavidin-HRP (R&D Systems) and washed to remove all unbound substrates. 50 μL/well of TMB color reagent (R&D Systems) was added to each well and incubated for 3-8 minutes until blue color developed. The reaction was stopped by adding 25 μL of 2N H_2SO_4 and absorbances measured on a plate reader (Biotek Gen 5.1.1) at 450 nm for signal and 570 nm for correction. Blank wells were averaged and corrected absorbances calculated for each sample using the formula (Measured450 – Blank450) – (Measured570 – Blank570). Raw absorbance values in the linear portion of the standard curve were converted to absolute concentrations in mg/mL, and fractions of high affinity antibody estimated as the ratio of antibody bound to NP_5 over that bound to NP_{25}.

METHOD DETAILS

We describe the construction of a model of B cell evolution within the germinal center, based on experimental parameters derived from the literature. The overall model consists of selection, fitness and mutation functions operating upon a population of B cells. Each of these modules is described in detail within the following sections.

Defining the B cell population undergoing evolution

As the core component of the model, we define the population of B cells undergoing evolution, denoted as the time-varying set B. During any given evolutionary cycle t, we define

$$B(t) = B_t = \{b\}_t \quad \text{(Equation 1)}$$

where b represents any B cell forming an element of the population set. See Table 1 for symbols used in modeling and equations.

We characterize the population of B cells firstly by its size, i.e. number of elements in the set, as

$$|B|(t) = |B|_t \quad \text{(Equation 2)}$$

and secondly by its distribution of receptor affinities. The set of affinities A is defined as

$$A(t) = \{\alpha_b | b \in B_t\} \quad \text{(Equation 3)}$$

where α_b represents the affinity of any individual B cell b present in the population B at cycle t. We then allow this population of B cells to undergo 40 cycles of evolution, from $t = 1$ to $t = 40$, estimated to correspond to approximately 3 weeks of antigen response.[18]

Initialization of the model by setting B cell population parameters

At $t = 0$, we initialized the model with a population of 50 founder B cells initiating the evolutionary cycle. This value was chosen from estimates of the number of clones seeding a typical germinal center, measured by Tas et al.[32]

Please cite this article in press as: Xiang et al., Phased fragility and stability of non-genetic B cell states in the germinal center accelerate the genetic evolution of antibodies, Cell Systems (2026), https://doi.org/10.1016/j.cels.2026.101590

$$|B|(t = 0) = |B|_0 = 50 \quad \text{(Equation 4)}$$

We assumed that the initial affinities of all the founders were normally distributed. We chose the mean of this normal distribution as a typical "low" affinity value, corresponding to an antigen-receptor dissociation constant $K_d = 10\mu M$.[33] This value can also be expressed on a linear scale, in terms of the free energy of binding ΔG between the antigen and receptor, using the relationship $K_d = exp\left(-\frac{\Delta G}{k_B T}\right)$ where $k_B = 1.38 * 10^{-23} J/K$ is the Boltzmann constant and $T = 310K$ represents body temperature in a warm-blooded animal. Thus, in terms of relative energy units, the mean affinity of the founder cells $\overline{\alpha_0}$ is fixed at $\overline{\alpha_0} = 11.5 k_B T$ where $1 k_B T = 4.3 \times 10^{-21} J$.

Further, we assume that the spread in affinity between these founder B cells is small, such that 99% of all cells have affinities within the range of thermal fluctuations, i.e. within $\pm k_B T$. Thus, we choose $3\sigma_0 = k_B T$, where σ_0 is the standard deviation of the founders' affinity distribution.

Overall, we assign the affinity of each founder B cell α_b by sampling values from a normal distribution with mean $\overline{\alpha_0} = 11.5 k_B T$ and standard deviation $\sigma_0 = 0.33 k_B T$, represented as

$$\alpha_b \sim \text{Norm}\left(\overline{\alpha_0}, \sigma_0^2\right), \ \forall b \in B_0 \quad \text{(Equation 5)}$$

Selection operating upon the B cell population

Selection of B cells arises from their interactions with antigen and follicular helper T-cells, with high affinity as the phenotype being selected for. Without capturing the minutiae of interactions, we instead develop an abstraction of this process, allowing modulation of the stringency of selection. We assume that T cell help is the primary driver of selection,[75] and is a limited resource partitioned across the B cell population based on their affinities. Thus, higher affinity B cells are more likely to receive T cell help, while lower affinity B cells receive none. We define the criterion for selection as a B cell having sufficient affinity to get T-cell help. In its simplest form, the probability of selection p_{Th} is given by:

$$p_{Th}(b) = H(\alpha_b - \alpha_{Th}) = \begin{cases} 0, \alpha_b < \alpha_{Th} \\ 1, \alpha_b \geq \alpha_{Th} \end{cases} \quad \text{(Equation 6)}$$

where H represents the Heaviside step function, such that only the B cells with affinities higher than a dynamic affinity threshold α_{Th} are selected while the rest are all eliminated.

We indirectly determine the value of α_{Th} at each cycle t, by prescribing the size of the population $|B|_t$ using experimental observations of germinal center size over time.[34] The threshold α_{Th} is chosen such that the number of selected B cells $\alpha_b \geq \alpha_{Th}$ matches this prescribed size. In cases where multiple B cells share the same affinity value exactly equal to α_{Th}, we randomly select a sufficient subset of these cells to ensure that the total number of surviving B cells equals $|B|_t$. We then update the set B to get:

$$B(t) = \{b \in B(t-1) | \alpha_b \geq \alpha_{Th}\} \quad \text{(Equation 7)}$$

$$\alpha_{Th} \text{s.t.} \ |B|_t = |B|_{exp} \quad \text{(Equation 8)}$$

The selected cells in $B(t)$ then undergo a cell fate decision between apoptosis, division, and plasma cell differentiation, with the progeny diversifying their receptor sequences through mutation, to complete the evolutionary cycle t.

Cell fate decisions and fitness in the subset of selected B cells

For the set of B cells that receive T-cell help and are selected, we then map their affinities to cell fate decisions (i.e. phenotype to fitness), based on the classical clonal selection theory.[43] The underlying assumption is that even among B cells that receive T cell help, the quantity of this help is partitioned based on their affinities. B cells on the lower end of the affinity distribution A receive only a little help and are more likely to die or divide a few times, while those on the higher end of A receive more help and are likely to expand further, or even differentiate into plasma cells at the highest affinities.

To model this, we first define a fitness score F_b^0 for each B cell, by transforming its absolute affinity α_b onto a common relative scale. Rather than using a rank-based cumulative distribution function (CDF) transformation, we compute F_b^0 based on the cumulative affinity contribution of selected cells. Specifically, we represent fitness score as the fraction of total affinity accounted for by cells with equal or lower affinity, such that for each B cell b:

$$F_b^0 = F_b^0(\alpha_b) = \frac{\sum_{j|\alpha_j \leq \alpha_b} \alpha_j}{\sum_j \alpha_j}, \forall \alpha \in A \quad \text{(Equation 9)}$$

where the numerator represents the cumulative affinity of all B-cells with affinity less than or equal to α_b, and the denominator normalizes this by the total affinity of the selected population. This transformation maps the affinity of each B cell $\alpha_b \in A$ with range

$[\alpha_{min}, \alpha_{max}]$ onto the fitness score $F_b^0(\alpha_b) \in [0,1]$, preserving the relative contribution of each B-cell to the total affinity-weighted selection pool.

We then partition this common range of fitness scores into a map of B-cell fate decisions, namely apoptosis, division, and plasma cell differentiation. We prescribe that fitness scores between correspond to apoptosis, since the experimentally measured apoptosis rate within germinal centers (excluding deaths due to both failed selection and lethal receptor mutation) is estimated around $p_{\text{death}} = 5\%$.[44] At the other end of the range, we prescribe that fitness scores between $(p_{\text{differentiation}}, 1$ undergo plasma cell differentiation, as the plasma cell differentiation rate is also estimated to be around $p_{\text{differentiation}} = 5\%$.[25,48]

Fitness scores in the intervening range $[0.05, 0.95]$ correspond to a clonal burst in the germinal center. Here, based on experimental observations,[45] B cells undergo a burst of multiple divisions varying between 1 to 8, with an average of 3 divisions. We assume that following each division, the progeny independently decides whether to divide again and produce another generation, or to terminate the burst at that generation. Hence, we partition the interval of fitness scores according to terminal generation in the experimental observation, by modeling the clonal burst over a range of generations, $G \in [1,8]$, having an expectation value $\langle G \rangle = 3$. The probabilities of reaching each terminal generation cumulatively set their corresponding thresholds of fitness score. In other words, the probability p_{G1} of terminating the burst after a single division is mapped to fitness scores in the range $[p_{\text{death}}, p_{\text{death}} + p_{G1}]$, a probability p_{G2} of dividing twice is mapped to $(p_{\text{death}} + p_{G1}, p_{\text{death}} + p_{G1} + p_{G2}]$, and so on until the eighth and last generation which maps the interval $(p_{\text{death}} + p_{G1} + \ldots + p_{G7}, p_{\text{differentiation}}]$. The resulting cell fate decision map is illustrated in Figure S6A, and detailed threshold values are listed in Table 3.

Finally, we assume that all B cell progeny that have reached their terminal generation re-enter the germinal center reaction for the subsequent cycle of evolution $t+1$. To conveniently capture the decision between cyclic re-entry and division at each generation of a clonal burst, we treat the 1-D cell fate map of terminal generations across fitness scores as the linear projection of a 2-D cell fate map, where the second dimension now represents generation number. Thus, at each generation, the fitness score threshold corresponding to that terminal generation now marks the boundary between cyclic re-entry and division. Using the above example to illustrate, the first generation maps fitness scores in $[p_{\text{death}}, p_{\text{death}} + p_{G1}]$ to re-entry and $(p_{\text{death}} + p_{G1}, p_{\text{differentiation}}$to division, the second generation maps fitness scores in $[p_{\text{death}}, p_{\text{death}} + p_{G1} + p_{G2}]$ to re-entry and $(p_{\text{death}} + p_{G1} + p_{G2}, p_{\text{differentiation}}$ to division, and so on until the eighth and last generation which maps the entire interval $[p_{\text{death}}, p_{\text{differentiation}}]$ to cyclic re-entry. This 2-D expansion of the cell fate decision map across generations is also illustrated in Figure S6A.

Following the assignment of cell fate decisions to each B cell b, we update the population B. Cells undergoing either apoptosis or plasma cell differentiation are removed from the population. The plasma cells are added to a separate set P (where we assume that there are no plasma cells prior to simulation, hence $P(0) = \varnothing$). The set of progeny $\{b_G\}$ from the terminal generation of a clonal burst are added to the population $B_t$and carried forward to the subsequent evolutionary cycle for selection. This modification of the population is represented as:

$$B(t) = \begin{cases} B_t \backslash \{b\}, 0 \leq \alpha_b < p_{\text{death}} \\ B_t \backslash \{b\} \cup \{b_G\}, p_{\text{death}} \leq \alpha_b \leq p_{\text{differentiation}} \\ B_t \backslash \{b\}, p_{\text{differentiation}} < \alpha_b \leq 1 \end{cases} \quad \text{(Equation 10)}$$

$$P(t) = P(t-1) \cup \{b\}, \alpha_b > p_{\text{differentiation}} \quad \text{(Equation 11)}$$

Stochasticity and non-genetic heritability of cell fate decisions

Stochasticity in cell fate decision making may arise as a result of intrinsic noise in the intracellular molecular network regulating cell fates. To model this, we introduce a stochasticity parameter S, defined as the degree of decorrelation between the affinity-dependent initial fitness score F_b^0 of a selected B cell, and the effective fitness scores F_b altered by noise at each generation of its proliferative lineage (Figure S6B). We define S as:

$$S = 1 - \rho(F^0, F) \quad \text{(Equation 12)}$$

where $F^0 = \{F_b^0\}, \forall b \in B_t$ and $F = \{F_b\}, \forall b \in B_t$ respectively represent the set of affinity-dependent and effective fitness scores for all B cells in the population, and $\rho(F^0, F)$ is the Pearson correlation coefficient between them.

To do this for each F_b^0, we draw the modified fitness score from a truncated normal distribution (restricted to the range [0,1] of possible fitness scores) around the mean value F_b^0. The spread of this distribution is given by a standard deviation σ_S which is determined by the desired degree of decorrelation S.

$$F_b \sim \text{TN}_{[0,1]}(F_b^0, \sigma_S^2) \quad \text{(Equation 13)}$$

To approximate the value of σ_S, we assume normality for the distributions of both F^0 and F. The Pearson correlation coefficient between them is given by

$$\rho(F^0, F) = \frac{\text{Cov}(F^0, F)}{\sigma_{F^0} \cdot \sigma_F} \quad \text{(Equation 14)}$$

We assume $F_b = F_b^0 + x_i$ where x_i follows the normal distribution

$$x_i \sim N(0, \sigma_S^2) \quad \text{(Equation 15)}$$

Thus, the mean of F remains unchanged since

$$\mu_F = \mu_{F^0} + \mu_x = \mu_{F^0} + 0 = \mu_{F^0} \quad \text{(Equation 16)}$$

The variance of F is given by

$$\sigma_F^2 = \sigma_{F^0}^2 + \sigma_x^2 = \sigma_{F^0}^2 + \sigma_S^2 \quad \text{(Equation 17)}$$

Hence the covariance between F^0 and F can be simplified such that

$$\mathrm{Cov}(F^0, F) = \mathrm{Cov}(F^0, F^0 + X) = \mathrm{Cov}(F^0, F^0) + \mathrm{Cov}(F^0, X) = \mathrm{Var}(F^0) \quad \text{(Equation 18)}$$

Since F^0 and X are independent, $\mathrm{Cov}(F^0, X) = 0$.

Therefore, we can substitute this in Equation 14 for the correlation coefficient to get

$$\rho(F^0, F) = \frac{\mathrm{Cov}(F^0, F)}{\sigma_{F^0} \cdot \sigma_F} = \frac{\mathrm{Var}(F^0)}{\sigma_{F^0} \cdot \sqrt{\sigma_{F^0}^2 + \sigma_S^2}} = \frac{\sigma_{F^0}}{\sqrt{\sigma_{F^0}^2 + \sigma_S^2}} \quad \text{(Equation 19)}$$

Therefore, we can determine σ_S based on the standard deviation σ_{F^0} of B cell fitness scores and the stochasticity parameter $S = 1 - \rho(F^0, F)$ by rearranging Equation 19 to get:

$$\sigma_S^2 = \frac{\sigma_{F^0}^2}{\rho(F^0, F)^2} - \sigma_{F^0}^2 = \frac{\sigma_{F^0}^2}{(1 - S)^2} - \sigma_{F^0}^2 \quad \text{(Equation 20)}$$

When cells enter a clonal burst, in the subsequent generations after the first, we also model a possible reduction in stochasticity due to non-genetic heritability among the progeny (Figure S6C). To do this, we introduce a heritability parameter h to modify the stochasticity to get $\tilde{S}$:

$$\tilde{S} = S \cdot (1 - h) \quad \text{(Equation 21)}$$

The value of h is chosen in the range $h \in [0,1]$, where $h = 1$ represents perfect inheritance of cell fate propensities, and $h = 0$ indicates a complete lack of non-genetic correlation. After each cell division, we update the fitness scores for progeny b' and b'' based on their parent b (Figure S6C), by modifying Equation as:

$$F_b', F_b'' \sim \mathrm{TN}_{[0,1]}(F_b, \sigma_{\tilde{S}}^2) \quad \text{(Equation 22)}$$

where $F_b{}'$ and $F_b{}''$ represent the fitness score of the progeny after this redistribution, and calculate $\sigma_{\tilde{S}}^2$ by modifying Equation 20 as:

$$\sigma_S^2 = \frac{\sigma_{F^0}^2}{(1 - \tilde{S})^2} - \sigma_{F^0}^2 = \frac{\sigma_{F^0}^2}{(1 - S \cdot (1 - h))^2} - \sigma_{F^0}^2 \quad \text{(Equation 23)}$$

Mutation in the subset of dividing B cells

B cells undergo somatic hypermutation (SHM), where the immunoglobulin locus undergoes point mutations that may alter the receptor sequence (genotype), and hence the receptor affinity (corresponding phenotype). This occurs only during divisions, and hence is confined to the subset of dividing B cells in each generation during a clonal burst. For each daughter cell, we assume that whether a mutation occurs or not can be modeled as a single Bernoulli trial with a mutation probability p_m. We use a value of $p_m = 0.5$, derived based on estimates of the rate of SHM (1 mutation/1000 bp in each division[36]) and the length of the immunoglobulin locus (600 bp[37]).

$$Bernoulli(p_m) = \begin{cases} 1 - p_m, \text{for no mutation} \\ p_m, \text{for mutation} \end{cases} \quad \text{(Equation 24)}$$

Once we determine that a daughter cell will undergo mutation, we next determine the impact of that mutation – whether it is synonymous, lethal, or changes the affinity of the cell. We assign the probabilities of each of these three outcomes to be 0.53, 0.28, and 0.19 respectively, based on theoretical estimates by Shannon and Mehr.[38]

Daughter cells that undergo synonymous mutations are left unchanged in the population. In the case of lethal mutations, we remove those daughter cells from the population of B cells.

$$B(t) = B(t) / \{b\}_{lethal} \quad \text{(Equation 25)}$$

Please cite this article in press as: Xiang et al., Phased fragility and stability of non-genetic B cell states in the germinal center accelerate the genetic evolution of antibodies, Cell Systems (2026), https://doi.org/10.1016/j.cels.2026.101590

Finally, if we determine that a daughter cell will change its affinity due to mutation, we sample the change $\Delta\alpha$ from a probability distribution determined previously,[39] where only 5% of mutations are advantageous and 95% of them are deleterious. We update the affinity for any daughter cell b' based on its parent b as:

$$\alpha_{b'} = max\ (\alpha_b + \Delta\alpha, \alpha_{min}) \quad \text{(Equation 26)}$$

where we set a minimum affinity limit $\alpha_{min} = 1k_BT$, to avoid non-physical values corresponding to purely stochastic interactions. This lower bound approximates the thermal energy scale, below which receptor–ligand interactions are dominated by Brownian motion and do not represent meaningful binding events.

Modulating the stringency of affinity-dependent selection

Selection of B cells is an inherently stochastic process, owing to random noise on both intracellular and intercellular scales. We attempted to capture some of this stochasticity in our model by considering a degree of decorrelation between the affinity of a B cell and its probability of selection. We thus introduced a stringency parameter K such that at $K = 1$ the selection probability is, as before, equivalent to the Heaviside step function, and at $K = 0$ the probability of selection is completely independent of affinity. We began by defining the updated probability of selection $\tilde{p}_{Th}$ as proportional to the logistic weight function w_{Th}:

$$\tilde{p}_{Th}(b) \propto w_{Th}(b) = \frac{1}{1+e^{-k\alpha'_b}} \quad \text{(Equation 27)}$$

where $k = \frac{K}{1-K}$ and α'_b represents a linearly normalized α_b such that affinities in the range $[\alpha_{Th}, \alpha_{max}]$ are mapped to $[0, 1]$:

$$\alpha'_b = \frac{\alpha_b - \alpha_{Th}}{\alpha_{max} - \alpha_{Th}} \quad \text{(Equation 28)}$$

Like α_{Th}, the value of α_{max} was determined at each cycle t:

$$\alpha_{max} = \max_{b \in B(t-1)} \alpha_b \quad \text{(Equation 29)}$$

Finally, to obtain concrete values for $\tilde{p}_{Th}$, we normalized our weights by a normalization constant c, such that the expected number of positively selected B cells was at most equal to the expected number of B cells for timestep t:

$$\sum_{b \in B(t-1)} \tilde{p}_{Th}(b) \leq |B|_t = c \cdot \sum_{b \in B(t-1)} w_{Th}(b) \quad \text{(Equation 30)}$$

Solving for c, we obtained:

$$c = \frac{|B|_t}{\sum_{b \in B(t-1)} w_{Th}(b)} \quad \text{(Equation 31)}$$

which yielded the following concrete expression for the updated probability of selection:

$$\tilde{p}_{\mathrm{Th}}(b) = min(c \cdot w_{\mathrm{Th}}(b), 1) \quad \text{(Equation 32)}$$

Simulation details

The model code was written and run using Python version 3.11.4 on an Ubuntu server across 64 processing cores. To ensure the reproducibility of insights obtained from these probabilistic dynamics, we performed Monte Carlo simulations, averaging results across multiple simulation runs for each parameter set. We determined the minimum number required to ensure reproducibility as 50 runs, using a bootstrap method where we initially performed a large number of runs, down-sampled them in successively lower proportions, and set a criterion of median within 1% to assess similarity between original and down-sampled affinity distributions. In practice, we performed twice the number, i.e. 100 runs per parameter set, to provide maximum confidence that probabilistic trends were accurately and robustly captured without ambiguity.

For the high-performance model, the code was written and run using Rust version 1.89.0, on the same Ubuntu server, also across 64 processing cores. In this case, to ensure reproducibility, we performed Monte Carlo simulations with 2000 runs per parameter set, assessed as above to provide higher confidence bounds that probabilistic trends were accurately and robustly captured.

QUANTIFICATION AND STATISTICAL ANALYSIS

Fitting stochasticity and heritability parameters to experimental measurements

To fit the stochasticity parameter, we utilized experimental measurements from Figure 5B in Mitchell et al.[16] by comparing the terminal generation distribution between experimental data and first-cycle simulation results using the Mann-Whitney U test. Additionally, we assessed lineage symmetry by applying a t-test to compare experimental lineage measurements from the same study (Figure 5A) with first-cycle simulation results. The data from both figures are summarized in Table S2. The statistical scores from

both U-test and t-test were normalized to a range of -1 to $+1$, and a combined model fitting score was computed as the average of both, to evaluate agreement between experiment and simulation. We conducted 100 Monte Carlo simulations using bootstrap re-sampling with 50 random samples per iteration. This process was repeated 300 times to obtain an average combined fitting score for each pair of stochasticity and heritability parameter values. Finally, we varied both stochasticity and heritability parameters to generate a heatmap illustrating the parameter space and its overall fitting.

Flow cytometry analysis to generate cell fate maps

Flow cytometry data were analyzed using FlowJo V10.0, with gating applied to identify lymphocytes, live lymphocytes, dead lymphocytes, and plasma cells (Figure S4A). The proliferation analysis tool was used to track cell generations and calculate population sizes for live, dead, and plasma cells. Target cell fate propensities were then derived using a set of mathematical equations, and presented in Table 3.

$$R_i = L_i - P_i \quad \text{(Equation 33)}$$

$$T_i = \varnothing_i + R_i + D_i + P_i \quad \text{(Equation 34)}$$

$$\begin{cases} D_i = \dfrac{T_{i+1}}{2}, \ if\ i = 0, \ldots, 7 \\ D_i = 0, \ if\ i = 8 \end{cases} \quad \text{(Equation 35)}$$

where $i \in [0, 8]$ represent B cell generations during clonal burst, R represents re-entering cells, L represents live cells, P represents plasma cells, T represents total cells, $\varnothing$ represents dead cells, and D represents dividing cells. This is based on the logic that the total number of cells in a subsequent generation must be twice the number of dividing cells in the previous generation, with the boundary condition that all cells in the terminal generation undergo either death, plasma differentiation, or cyclic re-entry. We constructed the expanded 2D-fate map as follows:

$$\begin{cases} T_{Xi} = \varnothing_i \\ T_{Ri} = \varnothing_i + R_i \\ T_{Pi} = \varnothing_i + R_i + D_i \end{cases} \quad \text{(Equation 36)}$$